A White Paper towards Sustainable Space Debris Recycling

Version 1.5 September 2022

Editors: Nick Klemz[1], C.A. Toomer[2]

with contributions from

Atilola Adegbite, Ahmed Alshobokshy, Taisia Bennett, Will Brown, Lucas Ferreira Ribeiro, Ivan Gomez, Mohit Joshi[3], Saif Majid, Kellan Reed, Jiang Ze Yeap, and Cheuk Him Yung

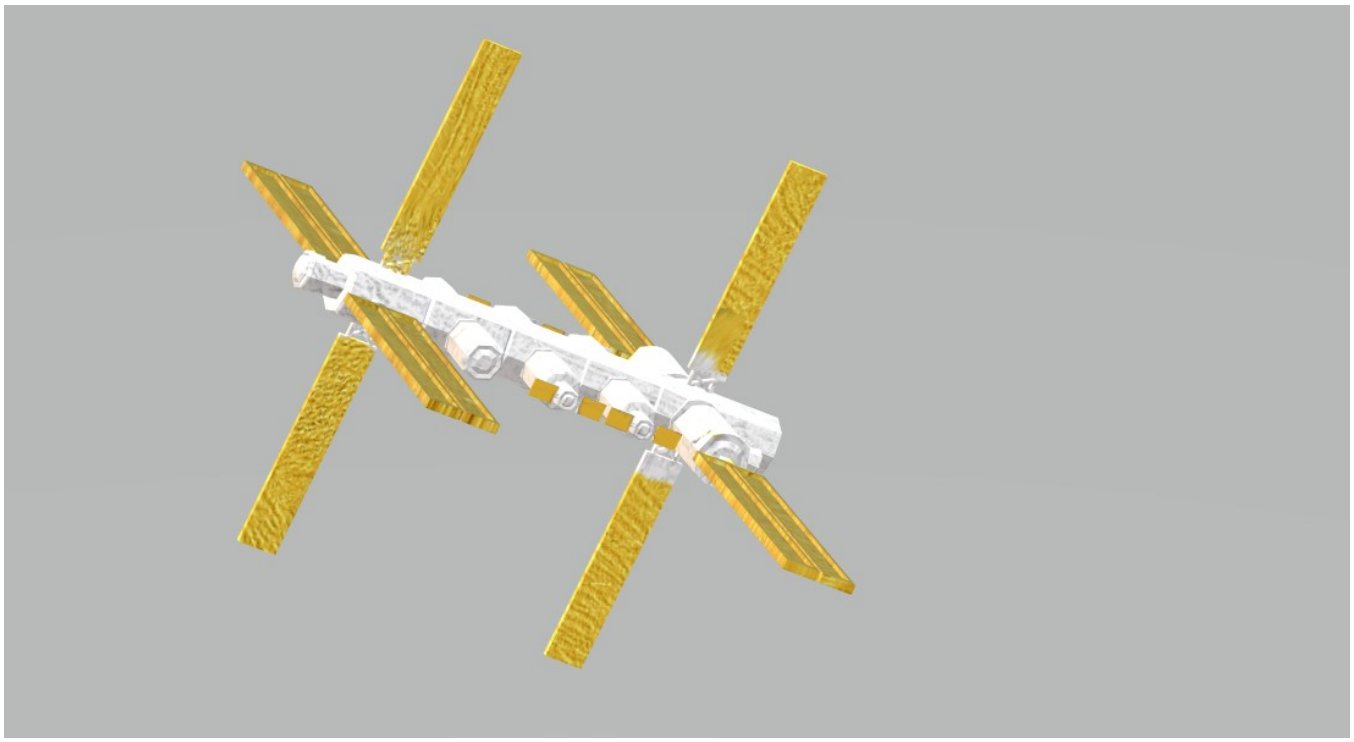

Figure 1: Conceptual Space Factory (Artist: Lucas Ferreira Ribeiro using Autodesk Maya and Adobe Photoshop)

Acknowledgments

The authors wish to acknowledge the support of the UK Space Agency and the SPRINT administrative team of the University of Leicester.

The Authors also wish to express their appreciation of the contract, research, finance and administrative teams of the University of the West of England for their assistance during this project.

1. Director, Field Reactors Ltd.

2. Associate Professor, School of Engineering, Faculty of Environment & Technology, University of the West of England, Frenchay Campus, Coldharbour Lane, Bristol BS16 1QY

3. Director, Interstellar Space Technologies.

Contents

1. Introduction

This white paper will constitute a roadmap of a suite of technologies that will be needed in the coming two to three decades to mitigate the problems of orbiting space debris and the wasteful practice of abandoning spacecraft which contain many rare and valuable materials.

The first section of the paper will describe how Field Reactor technology works and the second section will describe how Field Reactor technology could be used on Space Tugs (Figure 2), spacecraft designed to rendezvous and dock with other spacecraft for the purpose of on orbit servicing and boosting to new orbits. Although there have been several such experimental demonstrator spacecraft flown they have all suffered from the problem of finite propellant capacity.

The invention of the Field Reactor electric thruster (patent GB2588415 pending, (Klemz, 2019)) solves the problem of finite propellant capacity and it will enable entirely new types of mission profile all around the Solar system.

Field Reactor technology is at TRL3 and ready for immediate commercialisation. Spacecraft propelled by Field Reactors could be flown in just a few years.

The third part of the paper by the University of the West of England and Interstellar Space Technologies Ltd. will outline the technologies and techniques that will need to be developed to standardise spacecraft design to enable future craft to be recyclable on orbit, the recycling technologies that will be required, and a consideration of on orbit manufacturing. These technologies will require significant investment over timescales of two to three decades. The final part of the paper features a business analysis by Interstellar Space Technologies on the future of in-space manufacturing and recycling.

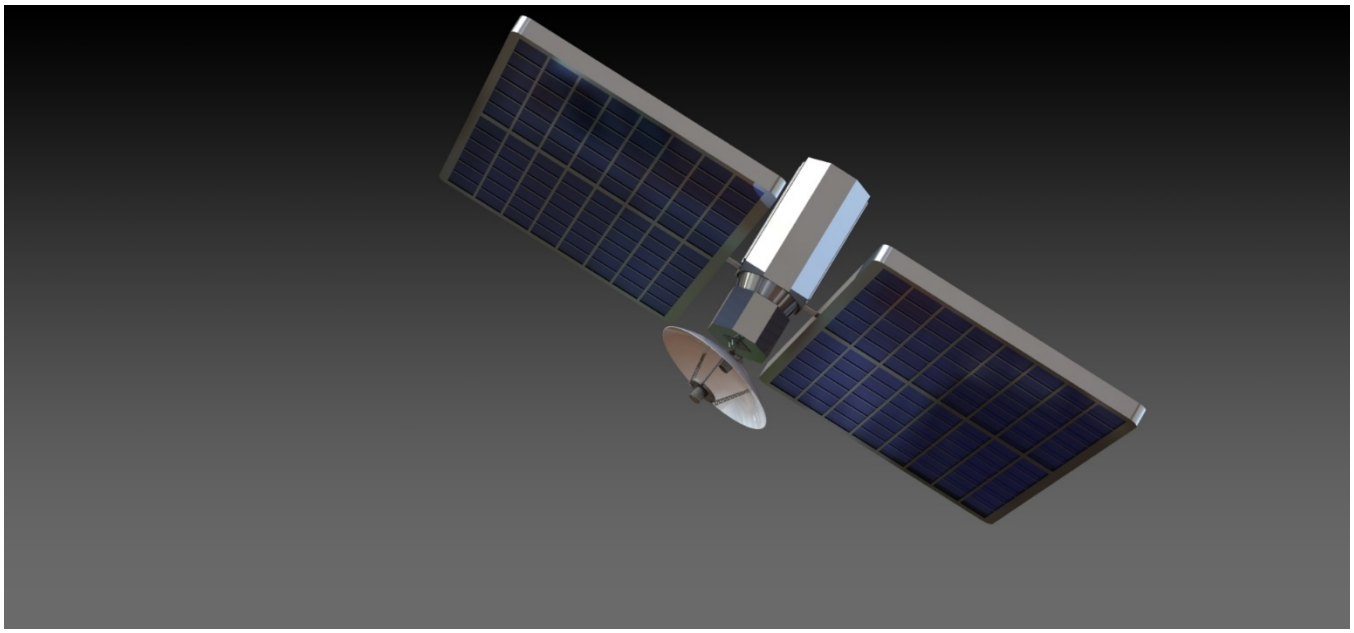

Figure 2 the Space Tug concept of Nick Klemz comprising a cylindrical field reactor, solar panels and communication disc. (SolidWorks: CAD designers Saif Majid, & Atilola Adegbite)

2. Space Debris

Space debris is a major topic for space-faring nations. There is estimated to be more than 9400 tonnes of debris in orbit with more than 28000 objects being tracked and an estimated 900000 objects of size from 1 cm to 10 cm and 128 million objects of size less than 1 cm (ESA, 2021). A report from ESA states "'Business as usual' space activities will lead to a progressive, uncontrolled increase in debris objects, with collisions becoming the primary debris source" (Fletcher, 2017). Space debris poses a real danger to spacecraft and astronauts and could make low Earth orbits unusable within decades. The OECD reports that up to 10% of total mission costs are currently dedicated to protecting spacecraft from space debris (OECD, 2020).

Many different approaches have been proposed for treating debris including deorbiting; reducing the orbital lifetime; moving spacecraft to lesser used orbits at end of mission; and active debris removal (NRCC, 1995). Identified methods for active debris removal include harpoons, nets, tethers, sling satellites, lasers, and claws. However, it was not until recently that funding towards developing the technology for missions to remove space debris have been tested with RemoveDebris (Forshaw et al, 2017) and further planned by ESA's ClearSpace-1 (ESA, 2019), JAXA's ADRAS-J (Forshaw 2018).

This project will introduce and investigate the idea of a "space tug" powered by a novel electric thruster, which would intercept debris items and boost them to a safe orbit or to an orbiting in-space recycling and manufacturing facility. A potential commercial case for it will also be highlighted.

3. The Field Reactor

3.1. Introduction

The Field Reactor is a novel electric motor and generator. As a motor it is intended primarily for use in spacecraft propulsion. This section of the white paper is a description of its operation by way of analogy and straightforward explanation. When people think about propulsion they generally think that something has to leave whatever is being propelled, that there has to be some kind of ejection in direct opposition to the propulsion.

All propulsion involves mass flow and the exploitation of the laws of conservation of energy and momentum. The goal of propulsion is to transfer the mass of the thing being propelled in the desired direction of travel and this is often achieved by exploiting a working fluid as a store of energy and momentum, which may be imparted to the working fluid one way and given to the mass being propelled another way. This is what happens in steam engines, internal combustion engines and jet propulsion. In electric motors, electric charge is used as a working fluid and is also seen as the mass analogue of the electromagnetic field.

The units of mass flow are kilogrammes per second, kg s^{-1}.

At the start of the Industrial Revolution the original working fluid used to power machinery was water and the energy and momentum it transferred to that machinery came from the Earth's gravitational field. Water may be used to move things in four main ways: imagine a log in the current of a river transported along with the flowing water; an octopus propelling itself forwards by ejecting a jet of water backwards; something being pushed away by the flow of water from a hosepipe; a surfer being pushed along by a wave.

The first three use the mass flow of water to carry the log along or to push the octopus or to use a jet to push something away.

However, in the case of the surfer there is no mass flow of water in the direction of the surfer's travel. The ocean wave being surfed is transverse; the displacement of the water is vertical, perpendicular to the direction of propagation of the wave and, as the changing gradient of the wave propagates, the wave is continuously destroyed and recreated in the direction of travel. And yet the wave transfers some of its energy and momentum to the surfer by the action of a force.

3.2 The Six Parameters of surfing

A skilled surfer balances the upward pressure of the rising wave against the combined weight of surfer and board. There are six important parameters to consider. The first three are the upward pressure of the wave, the pressure gradient in space and the rate of change of pressure in time. The other three are the net force acting on the surfboard, the momentum inherited by the surfer from the wave and the resulting mass flow of the surfer and board in the direction of the propagation of the wave.

So, on the one hand there is the momentum gained by the surfer by riding the wave and on the other hand there needs to be an equal change in the momentum of the wave in order to satisfy Newton's laws of motion. In inheriting energy and momentum from the wave the surfer shortens the lifespan of the wave.

There are many similarities between the language used in fluid dynamics and in classical electricity and magnetism and it can be useful to draw rough analogies between the two subjects but it is not always appropriate. For instance, nobody knows how to propel a spacecraft by moving the space surrounding the spacecraft itself, analogous to the log example above, and it is probably not possible in practice for a variety of reasons (Alcubierre, 1994)

Jet propulsion in space, in the form of rocket motors and electric propulsion such as Hall effect thrusters, is well known but suffers from the problem of finite propellant as the mass flow of the spacecraft is achieved by creating an equal mass flow of exhaust in the opposite direction. When there is no more propellant there is no more propulsion although the vehicle may of course continue to move through the vacuum of space with its acquired momentum.

However, there is no way to produce a purely electromagnetic analogue of a jet propulsion system so, instead, the Field Reactor works like the surfing example from before. Electric charge in an evacuated cavity in the device acts as the working fluid, and the mass of the device itself flows under the action of a force due to a pressure gradient in the electromagnetic field which is continuously destroyed and recreated in the direction of travel, analogous to the surfer's wave. The motion of the charge in the cavity is transverse with respect to the motion of the device as a whole and the device inherits a fraction of the energy and momentum of the charge in the cavity, just as a surfer inherits energy and momentum from the wave they are surfing. As it is purely electrically powered a Field Reactor will continue to produce a force for as long as it has a power supply. This frees it from the constraints of a specific impulse and makes possible mission profiles where the impulse achieved is constrained only by the energy available and the working lifetimes of its components.

3.3. The Six Parameters of electromagnetic surfing

The theories of electricity and magnetism were developed from the seventeenth century onwards, so to understand how the Field Reactor can achieve movement of an object we need to look first to Maxwell's equations and the Lorentz force. This will lead from classical electricity and magnetism (Panofsky et al, 1962) theories to the Maxwell stress tensor σ_{ij} and from there to the electromagnetic stress-energy tensor $\boldsymbol{T}^{\mu\nu}$ (units of pressure, Newtons per square metre, when all terms are expressed in S.I. units). Please refer to Appendix 1 to see these equations written explicitly. The tensor $\boldsymbol{T}^{\mu\nu}$ is built on the tensor σ_{ij} written in negated form in all nine pairings of dimensions x, y and z. At this stage the Poynting vector **S** = **E** x **H,** which tells us which way energy is flowing in the electromagnetic field, is used, where **S** is the Poynting vector, and **E** and **H** are the electric and magnetic field strength vectors respectively**.** By taking $E=mc^2$ (where E in normal typeface stands for energy, which is scalar, and is not to be confused with the vector **E**), the Poynting vector is divided by c to give a corresponding electromagnetic momentum density**.** In Appendix 1 in the electromagnetic stress-energy tensor this is written simply as $\frac{1}{c}S_i$ but is elsewhere written in other ways (Panofsky et al, 1962). As **S** is an energy term, when it is divided by c it has units of momentum, kg m s^{-1}.

Then a work term, often written simply as U but written explicitly in the top left corner of the tensor in Appendix 1, is added to balance the work terms in σ_{xx}, σ_{yy} and σ_{zz} and which completes $\boldsymbol{T}^{\mu\nu}$ and gives the trace, the sum of the terms diagonally from the top left to the bottom right of the tensor, a value of zero.

At this stage can be introduced the concept of creating a region of relative high or relative low pressure in the cavity, depending on the direction of the flow of the working fluid (electric charge), pushing or pulling the magnet at the end of the Field Reactor cavity.

By differentiating the tensor $\boldsymbol{T}^{\mu\nu}$ with respect to space we obtain the tensor divergence, which is the electromagnetic pressure gradient at each point in space at an instant in time, and the momentum density derivative has units of kg s^{-1}, being the units of mass flow.

And when $\boldsymbol{T}^{\mu\nu}$ is differentiated with respect to time the momentum density derivative has units of kg m s^{-2}, being the units of force.

Now that we have defined the six parameters of electromagnetic movement as in: pressure, pressure gradient and rate of change of pressure, and force, momentum and mass flow, it is necessary to find an arrangement of components which will generate a force in the desired direction and surf a transverse electromagnetic pressure wave. That is to say, all we need to do is invent the Field Reactor.

3.4. Field Reactor transducer

The Field Reactor works as a thruster and as a controllable resistance to an external force. The Field Reactor is an active bidirectional transducer. A transducer is any device which converts energy from one type to another. Examples include microphones, loudspeakers, motors and generators. A bidirectional transducer is one which has two modes of operation which are symmetrical in time. For instance, a moving coil microphone will work as a speaker when driven with an audio signal. A moving coil speaker will produce a current when the cone is pushed. The chief difference between the starter motor and the alternator of a car is the speed at which their rotors turn; in terms of the general arrangement of their parts they are similar. An active transducer is one which requires a power supply.

The Field Reactor exploits the same physical principles as any other electric motor, where an electric current in the rotor creates a magnetic field which exerts a force on a magnetic field from the housing, the stator, which causes the rotor to move relative to the stator. An electric motor can only work because the rotor is free to move relative to the stator.

In the Field Reactor the field coil of the rotor is replaced with a space charge, a cloud of electrons, accelerated in an evacuated cavity to form a vortex circulating around the axis of the device. Because this cloud of electric charge and the housing are not mechanically attached they are free to move relative to each other and the magnetic field generated by the motion of the space charge exerts a force on a magnetic field from the stator, just as in any other electric motor, but the arrangement of the parts causes this force to act along the axis, as a thrust, rather than around it as a torque. The vortex-like flow of the electrons works just like the a current flowing in a coil and the device works like a coil next to a bar magnet, with the electromagnetic field in the cavity acting as a region of high or low pressure relative to the magnetic field of the stator.

When the magnetomotive force between a bar magnet and a coil carrying a current acts to push them apart, or pull them together, the energy and momentum they gain as they accelerate comes from the electrons flowing in the coil which slow down due to an induced electromotive force, which reduces the current flowing in the coil and reduces the magnetic field (a measure of the momentum of the current) from the coil and reduces the magnetomotive force.

3.5. The action of the Field Reactor as a thruster from first principles

This is a step by step description to allow you to see how the Field Reactor produces a force and that energy and momentum are accounted for due to the conservative, symmetrical nature of electromagnetism. This assumes that the device is free to move; so you might consider it to be in

free fall in space, for instance. The Field Reactor joins the family of “crossed field” devices which exploit the behaviour of electrons in the presence of electric and magnetic fields with components at right angles to each other.

Figure 3 Is a diagram in side-elevation of the simplest topology of the Field Reactor, which is similar to the experimental proof-of-principle prototype. As explained later in this paper, production models will most often be of a slightly different arrangement, with the anode at the centre of the cavity, while working in basically the same way. With a central cathode the force produced is both along an axis and a moment, whereas with the anode at the centre the force is purely linear as is the case for an attractive force between two bar magnets. A bar magnet (either permanent or electromagnet) with poles P and Q abuts evacuated cylindrical cavity C. The end caps of the cavity are made from a magnetically permeable material such as soft iron or electrical steel and the cavity walls are made from a diamagnetic conductor (if the walls are to function as the anode) such as copper. Cathode K is mounted in the centre of the cavity and may either be a hot cathode designed to emit electrons by thermionic emission or a cold cathode made of a material which emits electrons readily by field effect. The flux B from pole piece Q threads through the cavity to the opposite end cap. Plate R is made of a magnetically permeable material and acts as a flux return to pole P to complete a magnetic circuit. Loop L serves as an antenna to allow excess electromagnetic energy to radiate from the cavity. In this case the wall A of the cavity is the anode. There is a large potential difference between K and A which gives rise to electric field E. (Here **E** is simply an arbitrary name for the field between K and A and is not to be confused with either E as an energy term in the equation $E=mc^2$ or the electric field strength vector **E** of classical electricity and magnetism).

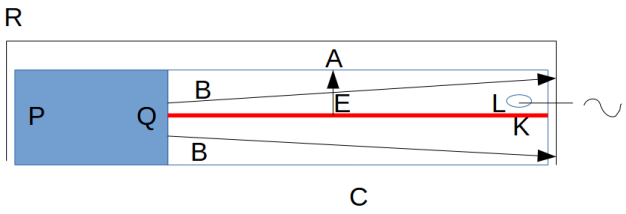

Figure 3. Field Reactor side elevation view (Nick Klemz, Kellan Reed)

We will now consider the case for a single electron emitted into the cavity by cathode K, as shown in Figure 4.

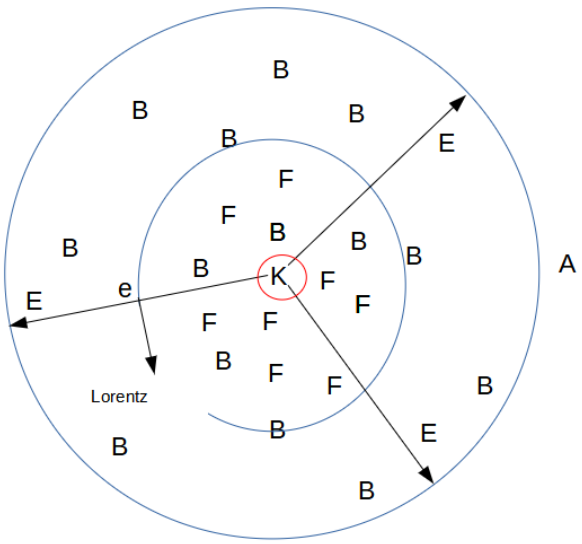

Figure 4. Plan view looking towards pole Q (Nick Klemz)

Magnetic flux, B ,is from pole Q and has a strong component along the axis of the cavity (in or out of the page) but the flux lines are not quite parallel, as is always the case from a pole piece.

Electron, e, with charge, q, is emitted from the cathode K and is accelerated radially towards the anode A by electric field, **E,** and its motion in the direction of **E** in the presence of **B** causes it to be acted on by the Lorentz force, **F**,

$$\boldsymbol{F} = q(\boldsymbol{E} + \boldsymbol{v} \times \boldsymbol{B})$$

where **v** is the instantaneous velocity of e. The Lorentz force causes the electron to accelerate at right angles to electric field **E** and magnetic flux **B** as indicated in the diagram.

Appropriate flux density of **B** and field strength of **E** are selected so that the Lorentz Force is equal to the centripetal force required to compel the electron to go around the cathode in a roughly circular path. This forms the simplest possible current loop which, by Ampere's circuital law, encloses a flux f of a density which is proportional to the magnetic constant (permeability of free space, m_0) and the beam current made by the motion of the electron as described by Maxwell's fourth equation in Appendix 1. Flux f may be seen as the relativistic component of the electromagnetic momentum of the moving charge: its density varies with rate of charge flow relative to the observer, magnet PQ. It is part of this momentum which is transferred to the body of the device by the action of a force.

As more electrons are emitted they follow similar paths around the cathode to form a vortex-like flow around the cathode with each electron adding its own component to flux f. This vortex-like flow of electrons in the cavity is equivalent to a vacuum core solenoid carrying a current which is the sum of all the individual current loops.

Due to the Lorentz force law, the direction of induced flux f is the opposite of flux B (flux F and flux B are disconnected) when the cathode is surrounded by the anode.

Thus there is a repulsive force between pole Q (flux B) and flux F which causes pole Q to accelerate away from the space charge in the cavity as the magnet and the space charge are pushed apart, as shown in Figure 5.

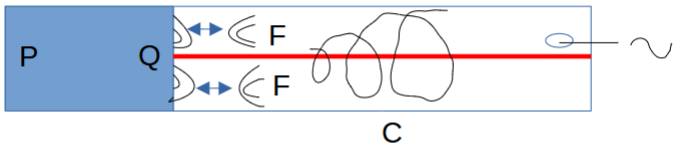

Figure 5 Side elevation showing vortex, fields and magnetomotive force pushing the fields apart. (Nick Klemz, Kellan Reed)

As pole Q moves relative to the space charge Faraday's law describes how the intersection of the flux B from pole Q with the paths of the moving electrons exerts an electromotive force (emf) on the space charge just as it would if it were moving relative to a coil carrying a current. Lenz's law describes how the sense of this emf is always such that it will cause a change in F which will tend to oppose the change being made by the relative motion of Q and the space charge. Please see Maxwell's third equation in Appendix 1. In other words, the acceleration of Q relative to the space charge will decelerate the electrons causing them to fall to the anode under the action of electric field **E** as the Lorentz force acting on them no longer matches the centripetal force needed to maintain a circular path and Q (and the rest of the housing of the device) will gain a proportion of the electromagnetic momentum the electrons lose as it accelerates relative to the space charge. The electrons slow down as they spiral away from the magnet and by the time they hit the anode they

have given a significant proportion of their electromagnetic momentum to the housing via the repulsive magnetic force between **B** and **F along the axis** so the momentum they have on hitting the anode, in a direction with a small component along the axis, is much less than they had when orbiting the cathode. **So there is a net thrust along the axis.**

All electromagnetic and mechanical momentum is conserved and accounted for. Momentum lost by the electrons as they decelerate tangentially is equal to the momentum gained by the housing as it accelerates along the axis. The device is mechanically sealed, but electromagnetically and thermodynamically the device is open as charge flows into the cavity via the cathode and flows out via the anode. Energy enters the cavity via the electric field **E** between cathode and anode and exits via the antenna as radio waves and as waste heat. The electrons in the cavity are effectively in free space and at the instant they are emitted from the cathode they have a velocity of zero, so all of the energy and momentum they gain is from the force due to the electric field **E** and they transfer this momentum to the housing via the magnetic field of PQ via the covariant electromotive (emf) and magnetomotive (mmf) forces as described by Faraday's law and Lenz's law.

These act orthogonally so it is perfectly legitimate for the device to accelerate along its axis as the electrons decelerate perpendicular to the direction of the device's motion.

Here Lenz's law is playing the role of Newton's third law. The emf acts in the opposite direction to the Lorentz force on the electrons and perpendicular to the mmf between flux B and flux F. The emf is opposite but not equal to the Lorentz force because of the action of the mmf along the axis and losses via loop L and waste heat, but all of the work done by the electric field E (the magnetic field component of the Lorentz force does no work) is equal to all of the work done by the emf, mmf and losses, and all of the momentum gained by the device as it accelerates is equal to the momentum lost by the electrons in the cavity as they decelerate under the action of the mmf and emf before hitting the anode.

This is the most important thing to understand.

Electrons are accelerated into the cavity continuously to replace the decelerated electrons which have hit the anode to rejoin the electric circuit, thus incrementally moving the electromagnetic pressure gradient through space as the whole device moves, as the space charge vortex is continuously destroyed and recreated, analogous to the transverse ocean wave being surfed described earlier in this document.

As the electrons move in the cavity they emit electromagnetic radiation which is an unwanted by-product of the process and needs to be removed from the cavity, to avoid overheating, via loop L and either absorbed by a load (in the prototype this is a block of polymer resin mixed with black copper oxide powder which was chosen for its absorption characteristics) or reclaimed.

3.6 In summary

To summarise, in common with other propulsion technologies, the Field Reactor works by exploiting the law of conservation of momentum. Most of the energy that goes into the space charge via **E** comes out via the loop L and as waste heat, with momentum being transferred from the vortex-like flow of electrons in the cavity to the whole device via the mmf between magnetic flux B and F. When working as a thruster then, the Field Reactor is essentially surfing a transverse, travelling, time varying electromagnetic pressure gradient and inheriting a small part of its energy and momentum in the direction of travel.

4. Applications of the Field Reactor

In this section we will look at how Field Reactor technology has the potential to transform the sustainability and economics of spaceflight, focussing on the particular application of Space Tugs in LEO and GEO but also mentioning the possibilities for very high impulse missions in and around the Solar system to achieve goals which are currently unattainable.

4.1 The Field Reactor as a damper or brake

We have seen how the Field Reactor works as a thruster by exploiting Faraday's law of induction and Lenz's law and that the vortex-like flow of electrons in the cavity is equivalent to a current in a vacuum core solenoid.

If the entire device is set in motion by the action of an external force then Faraday's law and Lenz's law again come into play as the relative motion of the magnet PQ and the space charge induces eddy currents and consequent magnetic flux in the space charge which tend to oppose the external force, thus damping or braking the motion. It is like the school experiment where a magnet is dropped down a copper pipe and takes a long time to come out of the bottom because of the braking action of magnetic flux due to eddy currents induced by the motion of the magnet relative to mobile electrons in the copper pipe, whereas a marble dropped down the pipe falls as expected.

Even if the potential difference between the cathode and the anode is zero and the space charge is not accelerated by **E** because **E**=**0** and an external force acts on the device the eddy currents induced by the relative motion of PQ and the space charge will produce a reactionary force and cause the emission of electromagnetic waves via loop L. Anode current will flow when electrons hit the anode as a result of being accelerated by the motion of the magnet relative to the space charge.

Thus, in acting as a brake or damper this transducer can harvest energy from whatever it decelerates. This is in line with expectations as a motor is a generator in time-reverse. The spectrum of the signal from the antenna carries information about its environment which would allow it to be used in novel sensing applications

By adjusting the flux density of **B** from magnet PQ (assuming PQ to be an electromagnet) and the potential difference between cathode and anode to vary **E** the characteristics of the Field Reactor may be tuned to suit specific requirements. It makes no difference if P and Q are North or South poles as with the cathode at the centre of the cavity the Lorentz force always ensures that the sense of the vortex-like flow of the electrons of the space charge is such that the magnetic flux enclosed by the current loops described by the individual electrons in the space charge is always repulsive to the pole Q.

4.2 Prototype versus working models

The previous section describes how the experimental prototype works, but working models will most likely be of the following configuration which has many advantages but which works in basically the same way. In this arrangement the cathode surrounds a central anode in the cavity. In this case, the electrostatic potential of the cavity wall would be held negative with respect to the cathode to force the electrons away from the wall and into the cavity towards the anode. In Figure 6 we see this arrangement. In this configuration the Lorentz force law ensures that the flux enclosed by the electrons circulating in the cavity is always of the sense that the force between Q and F is attractive and pulls magnet PQ towards the space charge.

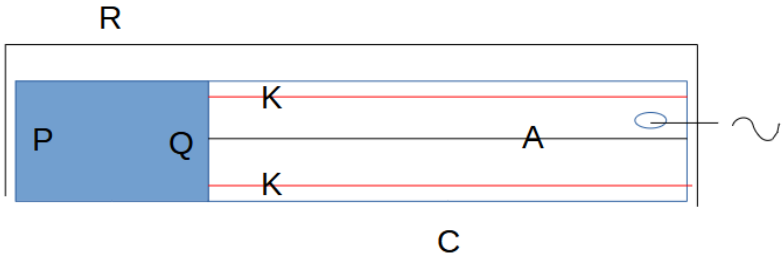

Figure 6 Side elevation with central anode (Nick Klemz, Kellan Reed)

In the prototype, with the cathode at the centre of the cavity, the region where the centripetal force and the electric field match and cause the electrons to circulate is relatively narrow as the flux F and B are disconnected and cancel out further away from PQ so the device works more like a diode and relatively few of the electrons contribute to making a force. With a central anode, however, flux B and F connect to form a magnetic circuit and add up so all of the electrons in the cavity contribute. For this reason, it is expected that production models will be of the central anode configuration and will have thrust to power and thrust to mass ratios orders of magnitude greater than the prototype. In this configuration the cavity could be made longer to produce a greater force. Many cavities may be machined in a single block to form a compact array and many electrodes may be in a single large cavity.

Both of the electrodes (anode and cathode) may be made as emitters with swappable roles to alter the characteristics of the device by altering the currents flowing through them and varying their electrostatic potentials.

Figure 7 shows a possible configuration where the cavity on one side of the magnet could be used with the central cathode (the “push” or repulsive configuration) and the other with the central anode (the “pull” or attractive configuration). Or they could both be “pull” or both be “push” which would give the effect of controllable inertia. With PQ as an electromagnet its polarity may be chosen at will.

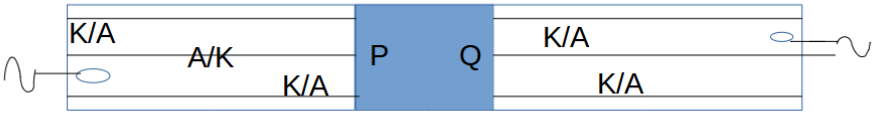

Figure 7 Side elevation with dual role electrodes (Nick Klemz, Kellan Reed)

4.3. The application of Field Reactor technology to Space Tugs for on orbit operations

Spaceflight has always suffered from the two problems of space junk and finite propellant. When a satellite runs out of propellant it becomes space debris, regardless of its operational status, with hundreds of millions of pounds worth of hardware entirely dependent on fuel worth just thousands of pounds. Space debris ranges in size from paint flecks to entire rocket stages. At orbital velocities even a fleck of paint poses a threat to small spacecraft.

Urgent action is required to prevent a “Kessler cascade”, (Kessler, 2009) where collisions between space debris make more debris leading to a situation where LEO is so full of debris that it becomes too dangerous to launch through the debris shell. Modelling has shown that the debris environment is already unstable, such that any attempt to achieve a growth-free small debris environment by eliminating sources of past debris will fail as debris will be made faster than atmospheric drag will remove it.

This is unsustainable.

Some companies, such as Northrop Grumman with its Mission Extension Vehicle are actively building Space Tugs. With two ongoing commercial missions (MEV-1 in 2020 and MEV-2 in 2021), SpaceLogistics is the first and only company to successfully perform on-orbit satellite servicing of commercial geostationary orbit (GEO) satellites (Anderson, 2021) but others, such as Maxar, which pulled out of an agreement with DARPA to work on the Robotic Servicing of Geosynchronous Satellites (RSGS) project, formed the opinion that on orbit servicing by Space Tugs to extend a satellite's lifetime is uneconomic for a private sector company but it is working on the NASA funded Restore-L mission which has the primary objective of refuelling the Landsat-7 spacecraft (Foust, 2019).

Airbus, part of The Consortium for Execution of Rendezvous and Servicing Operations (CONFERS) is starting the development of its O.CUBED Services, to offer space and on-orbit services, to operate in three market sectors: GEO Services, Logistics and Active Debris Removal, as part of its Internal Space Tug project.

As part of its vision for on orbit servicing Airbus, along with many other satellite builders and operators, has long been researching and developing automated rendezvous and docking (primarily for the ATV used as a supply vessel to the ISS) and orbital debris removal (the RemoveDebris and e.Deorbit up to phase B1 projects) (Ferreira, 2021).

The biggest obstacle to creating a viable business model for on orbit servicing and Space Tugs to boost recently launched satellites to GEO and then, at end of life, tug them to graveyard orbits to await the development of on orbit recycling and manufacture, is propellant. Propellant is actually fairly cheap as a commodity but extremely expensive to launch into LEO.

Although a few demonstrator missions have been flown (MEV, ELSA-d, SpaceDrone[5]) the need for orbital fuel depots and support services for a constellation of servicing satellites themselves makes the private sector business model unfeasible, and it is still generally seen as better to launch a new satellite than to launch a servicing satellite to extend the mission of an already aged one. Orbital fuel depots would be large repositories of highly explosive material and an accident would generate a large amount of debris with highly unpredictable trajectories, which would pose a serious risk to other spacecraft and possibly deny access to some orbits for many years.

Using Field Reactor technology would eliminate the need for orbital fuel depots.

Many propellants are also exceptionally toxic. When a spacecraft is being prepared for launch one of the final tasks is to fill its fuel tanks. The people who do this have to wear positive pressure suits and the whole operation is extremely hazardous. The adoption of Field Reactors would eliminate the cost and risk associated with these dangerous ground operations.

A typical apogee motor used to boost a satellite to GEO, such as the ArianeGroup S400-12 (SatCatalog, 2022), has a thrust range of 340-440N, has a qualified accumulated burn life of 8.3 hours and a qualified cycle life of 100 cycles. The chamber and nozzle throat are made from platinum alloy. The tanks and pipes needed to store propellant and deliver it to the engine are made from titanium. The nominal flow rate is 135g/s which equates to a fuel load of around 4000Kg. When that fuel runs out the mission is over. Replacing all of this extremely expensive hardware with Field Reactors would deliver significant reductions in spacecraft mass, cost, complexity and risk of component failure. On 7 April 2019, the propulsion system of Intelsat 29e developed a fuel leak which resulted in the total

loss of the spacecraft just 3 years into an expected 15 year mission and the creation of a cloud of debris (Intelsat, 2019).

Space Tugs equipped with Field Reactors instead of chemical rockets or ion drives such as Hall effect thrusters would not suffer from any of these problems as Field Reactors are purely electrically powered and require no propellant as reaction mass. A Field Reactor will produce thrust for as long as it can be supplied with electricity, which is available in abundance in the form of solar power. As well as replacing conventional thrusters, Field Reactors could also replace control moment gyroscopes, which are bulky and prone to mechanical failures. The Kepler planet hunting mission completed its primary mission in November 2012 and began its intended 4 year mission extension only for this to be cut short after two of its control moment gyroscopes failed and in August 2013 NASA announced that it was ending attempts to restore the spacecraft to full working order and would instead look into reassigning it to a new science mission (Johnson, 2017).

A constellation of Field Reactor Space Tugs could stay on orbit for decades. They could either be used as roving vehicles to rendezvous and service many spacecraft over their lifetimes or be used for mission extension, docking with spacecraft which have run out of propellant but which are otherwise in good working condition. A Space Tug would provide replacement thrusters for the remainder of the mission, before boosting the spacecraft to a graveyard orbit at the end of the spacecraft's lifetime and then being reassigned to a new mission.

Spacecraft propelled by Field Reactors would have much longer operational lifetimes, lower launch mass and complexity and greater reliability than current designs. Thanks to the very high impulse a Field Reactor can impart to a spacecraft entirely novel mission profiles will become possible. A fleet of Field Reactor craft could commute between Earth and the Moon and Mars, the asteroid belt and the outer planets, with no fuel costs. Not only will Field Reactor technology transform the economics and logistics of existing mission profiles and enable vast improvements in sustainability in space, but it will also bring hitherto unachievable asteroid mining and scientific sample return missions within the realm of possibility.

In summary, Field Reactor technology is fully sustainable, requiring no propellant, is physically very robust and capable of being engineered to give decades of continuous operation. Field Reactors will enable viable business models for private sector on orbit servicing and recycling and make possible entirely new markets in space.

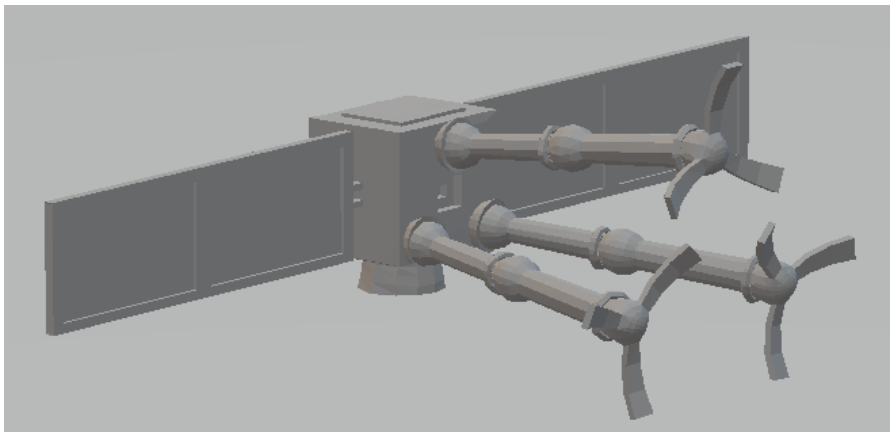

Figure 8 Artist's rendition of a space tug with its solar panels and the addition of 3 arms for grasping the debris (Lucas Ferreira Ribeiro, software Autodesk Maya)

5. Numerical Simulation Methods for a Field Reactor

5.1 Simplified Model - Solenoid

The simplest magnetic confinement configuration for a Field Reactor is in the form of a solenoid. The main role of the solenoid in the system is to be displaced in the opposite direction to that of the magnet which is also present. The displacement of both of these generate a zero net mechanical momentum. However, during this process, a force is generated from the electromagnetic momentum of the current present in the solenoid, which results in being proportional to the available current. It must be noted that as the magnet and solenoid move further apart, the current varies. This is due to the variation in voltage between the solenoid terminals varying with the electromotive force due to the displacement between both the magnet and solenoid.

The key difference when modelling the solenoid in the case of a Field Reactor in comparison to a regular solenoid, is the fact that the coils which are normally present in the solenoid are instead replaced by a space charge which consists of electrons. Thus, the main focus in the numerical simulation aspect is modelling the electron behaviour and the prescribed vortex motion the electrons experience.

5.2 Numerical Simulation Methods

5.2.1 Starfish and the Particle-in-cell method

In this section, the Particle-in-Cell (PIC) code which will be referred to for simulating the simplified model of a Field Reactor is Starfish. This is an open-source two-dimensional Electrostatic Particle-in-Cell (ES-PIC) code which has seen applications for plasma simulations and more specifically, in the field of electric propulsion (Brida, 2018) Particle velocities in Starfish are updated by using Lorentz force

$$\boldsymbol{F} = q(\boldsymbol{E} + \boldsymbol{v} \times \boldsymbol{B})$$

Several algorithms can be coupled in order to update the velocity, in the case of Starfish, it uses a combination of a Leapfrog integrator alongside a Boris scheme. Both of these have seen very successful applications in the field of electric propulsion modelling, and thus are suitable for this project (Brieda, 2018) The Lorentz force illustrates the effect an electric field and a magnetic field have on a particle, or in the case of this project an electron. An electric field accelerates a particle whereas a magnetic field will rotate the particle. This particle rotation is given by the cyclotron frequency:

$$\omega_c = \frac{|q|B}{m}$$

and the radius of the given rotation is given by Larmor's radius

$$r_L = \frac{v_\perp}{\omega_c} = \frac{m v_\perp}{\lfloor q \rfloor B}$$

where m is the mass of the particle, $v_\perp$ is the component of the velocity perpendicular to the direction of the magnetic field. Larmor's radius shows how the radius is inversely proportional to the magnetic field strength. The rotation that the particle performs is about the field line.

The Boris method is to be used as the particle pushing algorithm as it seen in standard algorithms used in other fields of plasma simulations. This algorithm is chosen over other algorithms such as Tajima's

implicit and explicit methods (Tajima, 2013) due to requiring fewer calculations, and thus being computationally more efficient. The Boris method is broken down into different sections as it is illustrated below:

Half-acceleration

$$v^{-} = v^{k-0.5} + \frac{q}{m} E \frac{\Delta t}{2}$$

First half rotation

$$v' = v^{-} + v^{-} \times \frac{q}{m} B \frac{\Delta t}{2}$$

Second half rotation

$$v^{+} = v^{-} + v' \times \frac{2t}{1+t^2}$$

Second half acceleration

$$v^{k+0.5} = v^{+} + \frac{q}{m} E \frac{\Delta t}{2}$$

When a magnetic field increases in strength in an axisymmetric domain, such as the one supported by Starfish, the force produced in the axial direction would be given by δz

$$F_z = -\mu \frac{dB}{dz}$$

where the magnetic moment is given by

$$\mu = \frac{\frac{1}{2} m v_{\perp}^2}{B}$$

The magnetic moment is of great importance in applications where there is a magnetic confinement. It has previously seen use in order to prevent electrons being ”lost” to wall surfaces.

When injecting the electrons into the domain, the initial velocity components should be sampled from the Maxwellian Distribution Function VDF at the desired temperature the electrons should possess. This method of determining the initial velocity is a popular approach in the field of electric propulsion (Brieda & Keidar, 2012) and is applicable for the model being studied in this project, as it has also been validated in a range of different fields of physics. Another important phenomenon which must be taken into account when simulating this system is the drift of the charged particles in an electromagnetic field. The resultant velocity from the cross product of the electric and magnetic field is given by

$$v_E = \frac{E \times B}{B^2}$$

It must be noted that there is also another kinetic code called Lynx which has been used to simulate electrons across magnetic field lines (Brieda & Keidar, 2012) The solver that both Starfish and Lynx would have to use for this particular application is believed to be the Poisson solver in order to resolve the present electric field. Both starfish and Lynx have the ability to apply the Poisson solver. A further advantage of using a PIC code is the fact that one can vary the specific weight of the

present particles in the domain and thus reduce the computational time, however at the cost of introducing numerical noise.

In the study from Brieda and Keidar (2012) it can be observed that another possibility would be to use both Lynx and Starfish combined. In this particular case, Lynx is used to only simulate the electron mobility on the set magnetic field lines. This approach was used in order to numerically simulate a Hall-Effect thruster. Regardless of the program used, there are two alternatives when modelling electrons. This involves either simulating them as kinetic particles or as a fluid. The first approach to be taken would be to model them as kinetic particles, however, it would be of great interest to investigate the effect it would have on the results simulating the electrons as a fluid.

5.2.2 Elmer

Elmer is an open-source multi-physics Finite Element partial differential equation solver. The solver includes several physical models, however, those of interest for this project would be the electromagnetic module, as well as the particle dynamics module. However, similar to Starfish, if a desired model needs to be added, it can be done in the form of plugins. Elmer has previously also seen application in the simulation of plasma generation devices, and can be further be seen its validity in Bondarenko et al. (2017) A flow chart illustrating the generalised steps normally taken in order to use Elmer can be seen in Figure 9 (Bondarenko et al., 2017).

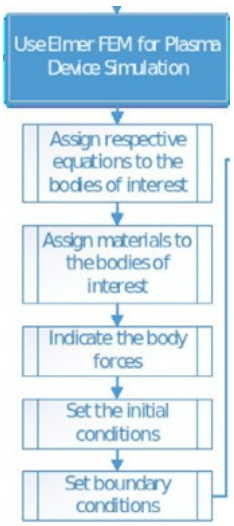

Figure 9: Elmer plasma simulation flow-chart (Bondarenko et al., 2017)

Elmer by default contains a module to handle three-dimensional magnetic Fields ”Magneto Dynamics”, by solving the Maxwell equations in an $\boldsymbol{A} - V$ form. The transient equations Elmer uses are similar to those Starfish uses. An alternative present in Elmer is instead of computing

Lorentz force in order to calculate the force exerted on a particle, the force exerted on a volume element can be utilized $\delta \boldsymbol{F} = (\rho \boldsymbol{E} + \rho \boldsymbol{v} \times \boldsymbol{B})\delta\Omega$. In the case of using the assumption that the electrons being modeled undergo collisions in a frequent manner, the current density of the electrons can be given by

$$J = \sigma\left(\frac{F}{q}\right) = \sigma E'$$

utilizing Ohm's law (Råback, 2013) The electromagnetic equations which would be valid over a region ω would be a magnetic version of Maxwell's equations which are illustrated from equations. (1a)-(1d).

$$\nabla \times E = \frac{-\partial B}{\partial t} \quad (1a)$$

$$\nabla \times \left(\frac{B}{\mu}\right) - J = g \quad (1b)$$

$$\nabla \cdot B = 0 \quad (1c)$$

$$\nabla \cdot J = 0 \quad (1d)$$

Elmer assumes plasma to be a hot ionized gas (Råbac, 2013) with the assumption of steady state magneto- hydrodynamics flow equations. This includes Faraday's law eq. (2a), energy conservation eq. (2b), flow continuity eq. (2c) and momentum eq. (2d). However, assuming the system that is being studied to be in a steady state, is a naive assumption and can therefore be said that it may not be a valid assumption. This is mainly due to the system's highly dynamical nature thus, directly affecting the velocity distribution in the given domain.

$$\nabla \times E = \frac{-\partial B}{\partial t} \quad (2a)$$

$$\frac{\partial E}{\partial t} + v.\nabla E = \nabla .\Theta + \left(\mu \nabla .v - \frac{2}{3}\mu \nabla .v\right)v + \rho_q E \times v \quad (2b)$$

$$\frac{\partial \varrho}{\partial t} + v.\nabla \varrho = 0 \quad (2c)$$

$$\frac{\partial(\rho v)}{\partial t} + v.(\rho v) = -\nabla p + \mu \nabla^2 v - \nabla\left(\frac{2}{3}\mu \nabla .v\right) + \rho_q (E + v \times B) \quad (2d)$$

The methodology used by Elmer can be summarised as solving the Navier-Stokes equations, alongside the magneto-hydrodynamics principles. This is not entirely practical as previously described. However, this can be modified by instead of utilizing the Navier-Stokes equations modelling the flow as charged particles similar to Starfish and following particle dynamics, which is a module already implemented in Elmer. The already present model "Particle Dynamics" would also have to be slightly modified in order to account for the interaction between charged particles.

5.2.3 Comparison

The working mechanism of Starfish and Elmer have been described in the above subsections, alongside with other principles that should be implemented into each individual code respectively in the form of plugins. the main benefit Elmer possesses over Starfish is the fact that it already currently

supports three-dimensional domains, however, this can be changed in Starfish by further extending the fundamental equations which are already embedded into the code. Other factors that also benefit Elmer is the fact that it takes a Finite Element Method approach, and thus is able to be used on an unstructured mesh if required. However, on the other hand, Starfish benefits from being a pure kinetic code instead of taking a fluid approach, as a kinetic code will allow the velocity distribution function of the electrons to evolve naturally throughout the simulation, unlike a fluid approach, which states assumptions regarding the velocity distribution functions shape. This as a result would in theory produce a more accurate result. Aside from the points previously established, Starfish has seen a higher use in the field of plasma simulation, more specifically for ion and hall effect thrusters in comparison to Elmer. Further showing the validity of the fundamentals currently established in Starfish.

5.3 Conclusion and Future work on expanding the model

To sum up, out of both of the codes described in this report, the most suitable one in order to model a simplified model of a Field Reactor would be Starfish, whilst adding the corresponding equations and algorithms described in the Starfish subsection of this report. However, a better alternative to using Starfish that would also have the benefits of both codes would be to develop a 3-D Finite Element Particle-in-Cell code (FEM-PIC). This is believed to cover all areas required and would follow the same physical principles as those discussed in the Starfish section, whilst also supporting an unstructured mesh. The downside of this alternative is time, as a significant amount of time would have to be spent on building this code instead of just developing plugins for Starfish or Elmer. This FEM-PIC code would also be highly adaptable to future versions of the Field Reactor.

A future evolution of the simplistic model of a solenoid reviewed in this report would be to model a cavity magnetron. This is of great importance to model this in a near future, as it would serve as a validation to the physical experiments that have been carried out, where a cavity magnetron is also used, as this exploits the similarities between the charge flow and the current in a solenoid.

6. In-Space Manufacturing

Activity is space is expected to continue to increase over the next decade and beyond. For example, Morgan Stanley estimate that the global space industry will increase from $350 million in 2016 to $1 trillion by 2040 (Morgan Stanley Space Team, 2022). A significant part of these future profitable activities will be in-space manufacturing. According to the ISECG Global Exploration Roadmap (ISECG, 2018), availability of future space platforms will be required for Government and private organisations for in-space manufacturing. This is in line with ESA's Terrae Novae 2030+ Strategy roadmap (ESA, 2022) which envisions SciHab (Science & Habitation) platforms owned and operated by commercial entities for a number of purposes including in space manufacturing. Although estimates on the value of in-space manufacturing vary, the consensus is that there will be a continual growth to 2030 and beyond.

In-space manufacturing is initially expected to mainly cater for products and services to be used on Earth, in 2019 this figure was around 95% (Weinzierl, Matt & Sarang, Mehak, 2021), However as the space sector stabilises its operations into a continual commercial presence in space, there will be opportunities to expand the customer base more to space based activities such as creating new modules, and space trusses. The in-space manufacturing activities include 3D printing, pharmaceuticals, bio-technology, material science, fluid physics, fibre-optic cables, microchips,

7. Recycling in space

Recycling in space has generally been for maintaining and extending the lifetime of a space mission where humans are on-board. Thus recycling of air and water in a space station is well established and has the advantages of mission cost-effectiveness, sustainability and waste reduction.

However, the idea of reusing and repurposing defunct spacecraft, i.e. space debris, has been discussed for around a decade (Barnhart & Sullivan, 2012). Thompson et al. (2018) proposed a design for an in-space factory module to accept space debris, deconstruct the debris, take certain metal types for melting in which to produce metal wire for in-space 3D printing new products. The advantage of recycling space debris is that it would remove much of the space debris in low Earth orbit; prevent the subsequent build-up of debris from current spacecraft; provide a source of material for 3D printing in-space and reduce the cost of sending up new material from Earth. Recycling would repurpose some of the material instead of it finally burning up in the upper parts of the atmosphere.

8. Factory in space

8.1 Introduction

The concept of the factory in space is that it would be a semi-autonomous automated production line taking in material to be converted to useful products for use in space and/or on Earth. The factory would operate more efficiently if it was sustainable in terms of power using Solar panels or energy beamed to the factory from solar panels; receives material from in-space sources rather than from Earth and uses robots to perform the needed tasks. The factory would require tight cyber-security due to its tele-operation from e.g. a space station to which it may or may not be connected, and from control centres on Earth.

The concept described below (figure 10) is one of many that could be created. The scenario is that this factory is new and very recent so requires part construction on Earth which is then delivered to Space via conventional rockets. The factory module, robots and processing machinery would all be delivered in this manner. Future factories will be partly manufactured in space reducing the need for supply from Earth.

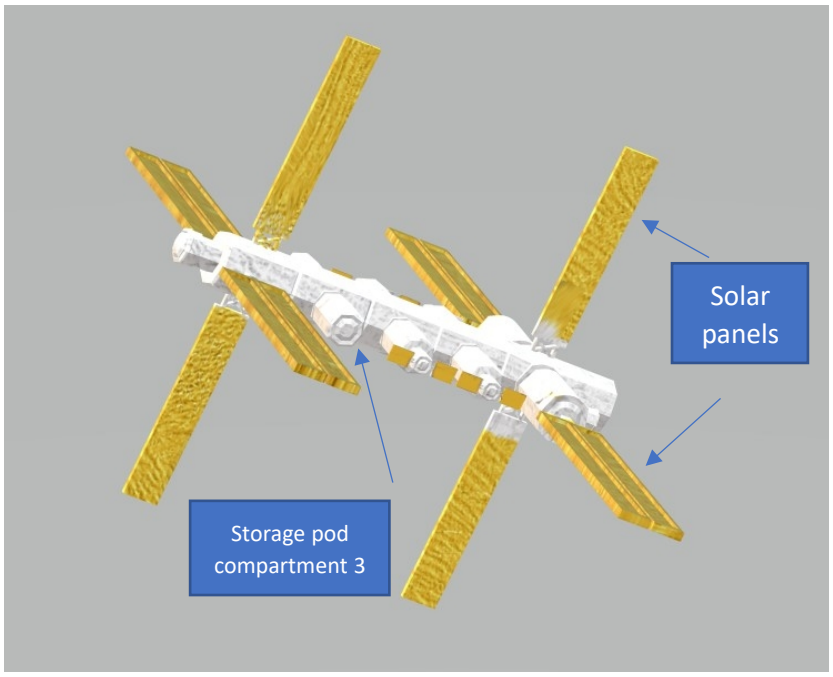

Figure 10 Concept for a space factory (Mohit Joshi & Lucas Ferreira Ribeiro) Software Autocad Maya and Adobe Photoshop

The factory will be compartmentalised by function and operate in the vacuum of space.

1. Using the space tugs from workpackage 2, the first compartment of the factory receives space debris at one end of the factory. The debris is then passed to compartment 2.
2. The second compartment houses the robots which deconstruct the debris. They receive the debris objects in sequence, deconstruct and separate into parts.
3. Those parts that are not used in this current factory are stored in external pods (compartment type 3) according to their size and composition (this material will be used later by other factories or operations).
4. The parts that are useful are conveyed to compartment 4 where the metal melting equipment is housed. In this compartment the chosen metal is melted and shaped using

electromagnetic fields so that metal wire of a specified diameter can be drawn and spooled. This metal wire can also be stored ready for later use. This procedure was proposed by Thompson et al (2018) and is currently being prototyped by a research group at Colorado School of Mines (Colorado, 2021).

5. Compartment 5 houses the 3D metal printing equipment where the recycled wire is used to create metal pipes, bars and connectors for a space truss using additive manufacturing techniques. Metal 3D printing is due to be tested on the ISS in 2023 from a mission by Airbus (Airbus, 2022).
6. Compartment 6 houses the various robots used to take the truss components from the previous compartment and take these components outside of the factory where they are assembled into the final structure.

Each of the operation of the compartments is described in the next sections. However before the factory is described, the aspect of the importance of robotics in collecting the debris is first considered.

8.2 Robotics and its use for Debris Capture and the space factory

The aim of recycling in space is to make operations more sustainable and cost-effective by reusing existing spacecraft and rocket material. In order for the space debris to be delivered to the factory, firstly the debris must be caught. Debris capture is a difficult task. Debris continues to belong to the original owner and collecting a piece of debris would require the owner's permission. In the future, there may be a requirement for the owner to organise the disposal of all of their debris above a designate size. Thus debris removal may become a commercial activity. The dangers of collecting the debris are numerous: failing to contain the debris and losing the object such that it takes a different path; parts of the debris object breaking up creating more debris; hazardous waste onboard the debris. Substantial insurance is needed so that initially debris can only be collected as part of an international effort.

As mentioned in section 2, there are many proposed approached to capturing debris. Which approach is better is not a part of this part. We have adopted a set of "grabber" robotic arms to illustrate the point of collection and delivery. A number of developing technologies are required including computer vision, feature recognition, tactile robotics, neural networks and AI algorithms to enable learning a more effective procedure. Robotics is an essential subject in the successes of debris collection and the space factory, and there are many aspects to research which will take decades before we have practical tested working systems . In this project some of the more immediate challenges in robotics have been studied. The robotics research was conducted by Jiang Ze Leap (his report is in Leap, 2022) who sought to answer the following points for debris collection and the space factory:

1. To study and implement a comprehensive robotics system that achieves the goals of debris collection and in the various automated tasks in the space factory.
2. To implement suitable machine learning algorithms in vision for object detection work.
3. To solve the inverse kinematics problem of the robotics arm to achieve desired position
4. To consider the deliverables and tasks of the factory for the placement of robotics arm.

The robotics architecture for both the debris capture and the subsequent delivery at the door of the space factory is presented in Figure 11.

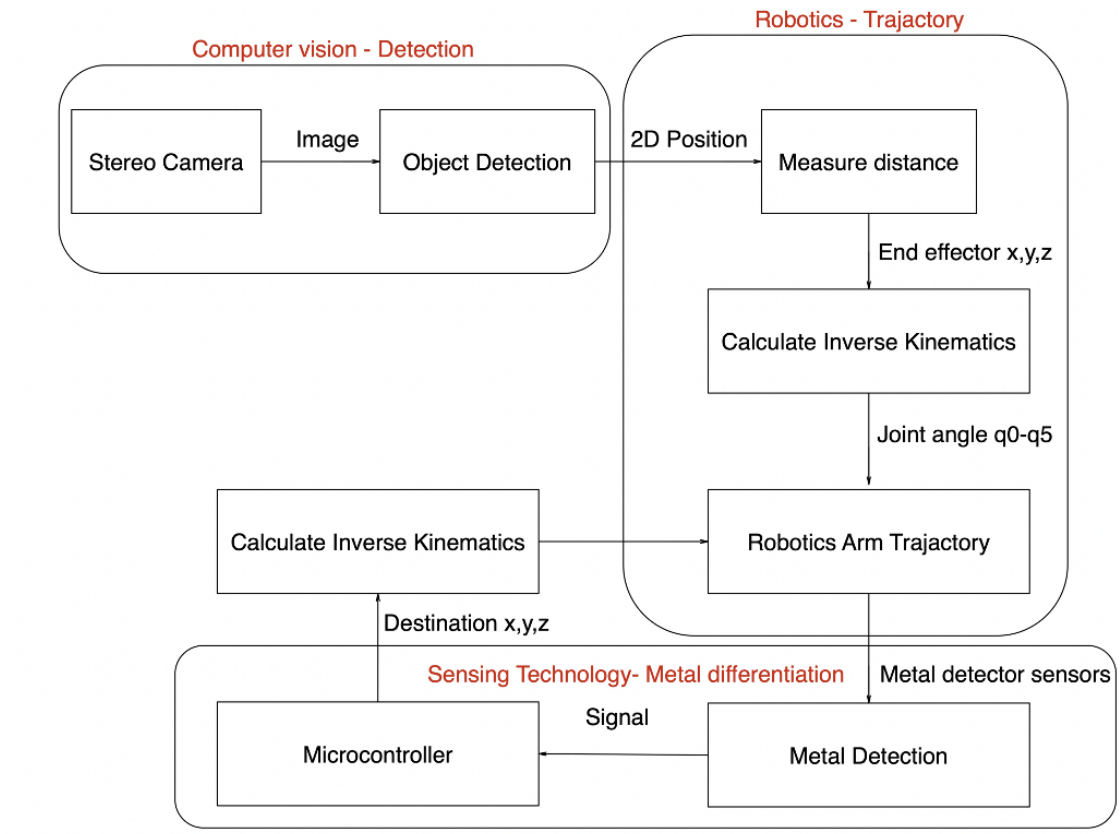

Figure 11. Robotics Architecture (Jiang Ze Yeap)

The robotics system architecture can be classified into three sections: computer vision for object detection, robotics trajectory and sensing technology for metal detection.

8.2.1 Camera Detection & Distance measurement

Computer vision in cameras is crucial for debris capture. Based on Figure 11, the detection approach chosen is the Convolutional Neural Network (CNN) using 2D vision of a debris image. CNN is a type of Artificial Neural Network (ANN) (Figure 12) that contains **multilayer perception (MLP),** which is made of many layers of input data to predict a predefined output data (Chintarungruangchai and Jiang, 2019). So this is a specialist approach for analysing images of the debris.

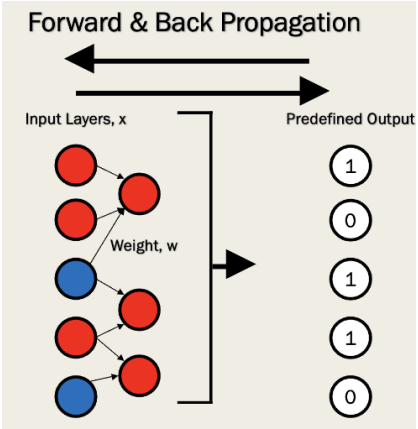

Figure 12: Structure of ANN consists of input layers x, weight, w, hidden layers, and predefined output (Chintarungruangchai & Jiang, 2019)

The output function, f, of an ANN structure can be concluded as follows:

$$f\left(\sum_i \left(w_i x_i + b\right)\right)$$

where, w is the weight, x is the "input layers" and b is the bias value.

Chintarungruangchai and Jiang (2019) state that CNN includes convolutional layers to make up the structure of ANN as input data, x. The kernel of the CNN also represents the weight of the structure, w (Figure 13)

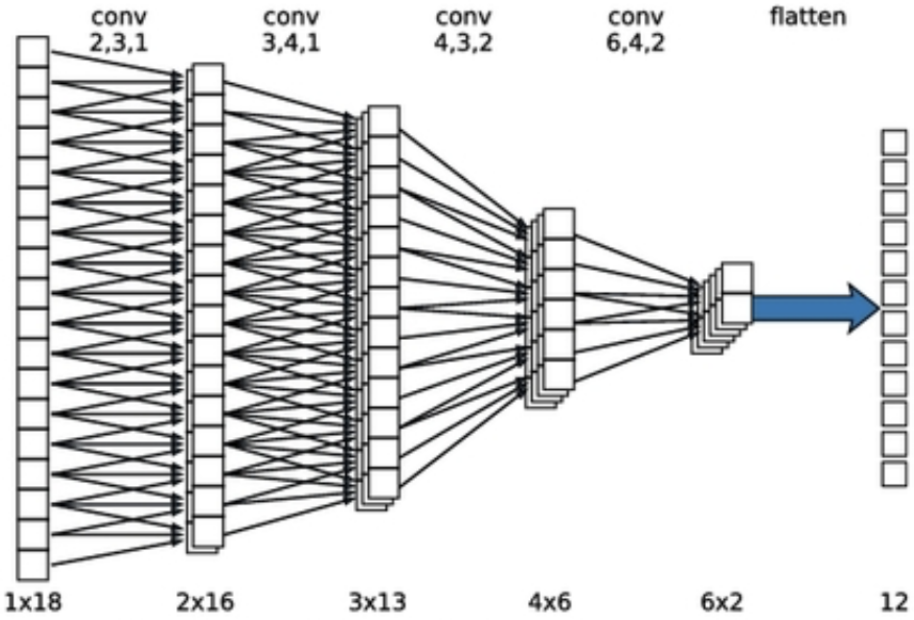

Figure 13: Example of structure of convolutional layers of 1D- CNN. The number at the bottom is channel number x data number in each layer. The numbers over the output channel number, kernel size and stride, respectively (Chintarungruangchai and Jiang , 2019).

As an example of how debris could be identified through computer vision feature detection, an open-source object detection method, You Only Look Once (YOLO) was implemented (GitHub, 2022).

Initially the model was taught to recognise 3D circular shapes, and then trained to distinguish between a disc, cylinder and a doughnut. The machine vision program establishes the contours of the shape and thus the dimensions and volume of the object. Where shapes have similar contours then there can be confusion and thus the machine learning needs to be continued until the training succeeds in being more accurate in identification or in recognising that more information is needed (a different viewpoint) until there is enough to make the distinction. This information is then conveyed to the robot arms so that the object can be successfully grasped.

The algorithm was then trained with 100 copyright free images from Google.com and bounding boxes are drawn to locate the position of a satellite. Figures 14 shows three of the correctly detected satellites (proven by the red box containing the satellite).

The space tug capture arms (Figure 8) are made of a sequence of joints to enable a flexible orientation. A gripper is included at the end of each arm. Each arm receives coordinates about the debris from the machine vision camera. These coordinates are used to create the inverse kinematics from which the positions of the effectors at the end of each robot arm can be obtained. The robot arm then moves and the gripper makes contact to secure the debris object. Due to the complicated

dynamics of the debris, this capture would be over a time period with the robot making successive adjustments.

Figure 14: Examples of where a satellite is detected (i.e. the red box) in image.

When a 2D position of an object is detected by a camera, a point cloud data from the stereo camera and the pixel at the selected 2D position can be known (Onishi et al., 2019). The Depth of Field (Figure 15) is an important factor to calibrate with the specification of the camera to obtain accurate 2D distance from camera to object (Adams and Willett, 2010).

$$D_{TOT} \approx \frac{2NCU^2}{f^2}$$

- where
  - N is F-number of lens
  - C is circle of confusion (on image)
  - U is distance to in-focus plane (in object space)
  - f is focal length of lens

Figure 15: Formula provided for Depth of Field (Adams and Willett, 2010).

Distance from the space tug to the debris object would then be evaluated using camera and lidar (Onishi *et al.,* 2019). The 3D reconstruction (by either Lidar or a stereo camera) is required to perform a triangulation from parallax between right and left images to obtain 3D position of the pixel image to measure the distance accurately. The grasping is a particularly difficult procedure in reality as the debris object may be tumbling and may be suffering in parts from fatigue. Thus grabbing the object could create the situation where the debris object breaks up and more debris is produced. It is thus advisable that part of the debris capture procedure is to locally analyse the state of the debris before capture is initiated.

8.2.2 Determining the robot arm movement using inverse kinematics

When a desired position is known in real-life, but the orientation and the end point where the robot must reach is unknown, is commonly identified as an inverse kinematics problem (Ning, 2021). Given the end-effector position is represented as T_n^0, the orientation can be recognised by finding the joint displacement angle, which is the angle of each axis on the robotics arm (q_1, q_2, q_3, …q_n), where n is the number of axes. The equation is determined as followed:

$$q = f^{-1}¿)$$

Where, q is the joint displacement angle, f^{-1} is the inverse kinematics function and T_n^0 is the end effector position.

In this project, the robot arm was chosen to have 6 axes with 5 degrees of freedom.

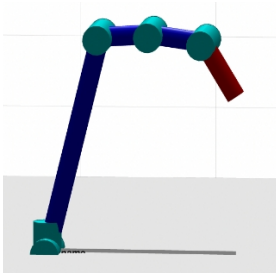

Figure 16: The example robotic arm of 6 axes and 5 degrees of freedom. The reference frame of the robotics arm was created in MATLAB. The red part represents the length of the claw to grab the satellite. (Jiang Ze Yeap, 2022)

The Denavit-Hartenberg (DH) is an organised and effective way to set reference frame for a robotic arm (Ning, 2021). Therefore, a DH table is created to visualise the 6-axis robotics arm (Figure 17).

d1 = Axis 1 to 2
d2 = Axis 2 to 3
d3 = Axis 3 to 4
d4 = Axis 4 to 5
d5 = Axis 5 to 6

a_n = z_{n-1} to z_n along x_n
α_n = z_{n-1} and z_n about x_n
d_n = x_{n-1} to x_n along z_{n-1}
θ_n = x_{n-1} to x_n about z_{n-1}

i	ai	alphai	di	thetai
1	0	pi/2	d1	q1
2	0	0	d2	q2
3	d3	0	0	q3
4	d4	0	0	q4
5	d5	0	0	q5

DH Table (conventional)

```
%% Joint Lengths (Inches)

d1= 40.25;
d2= 157;
d3= 38;
d4= 40;
d5= 45;
```

Figure 17: On the left is a Denavit-Hartenberg table using conventional method created in PowerPoint. On the right are the joint lengths chosen for an example robot arm (Jiang Ze Yeap, 2022)

The DH notation table is the relationship between the links of axes of n and (n+1). Therefore, the homogeneous transformation matrix of the DH notation is:

$$ {}^{n-1}\boldsymbol{T}_n = \begin{bmatrix} C_{\theta_n} & -S_{\theta_n}C_{\alpha_n} & S_{\theta_n}S_{\alpha_n} & r_nC_{\theta_n} \\ S_{\theta_n} & C_{\theta_n}C_{\alpha_n} & -C_{\theta_n}S_{\alpha_n} & r_nS_{\theta_n} \\ 0 & S_{\alpha_n} & C_{\alpha_n} & d_n \\ 0 & 0 & 0 & 1 \end{bmatrix}, $$

Figure 18 The transformation matrix needed to describe the sequential movement of the robot arm into the required position.

Where S=sine function, C=cosine function, alpha and theta are angles whose values are given in Figure 17. The robotics toolbox in MATLAB (Corke, 2022) is used to solve the inverse problem and produce the sequence of values for the joint displacement angles, q, so that the movement of the robot arm can be operated from the initial position into the final required position (e.g. to capture the debris object).

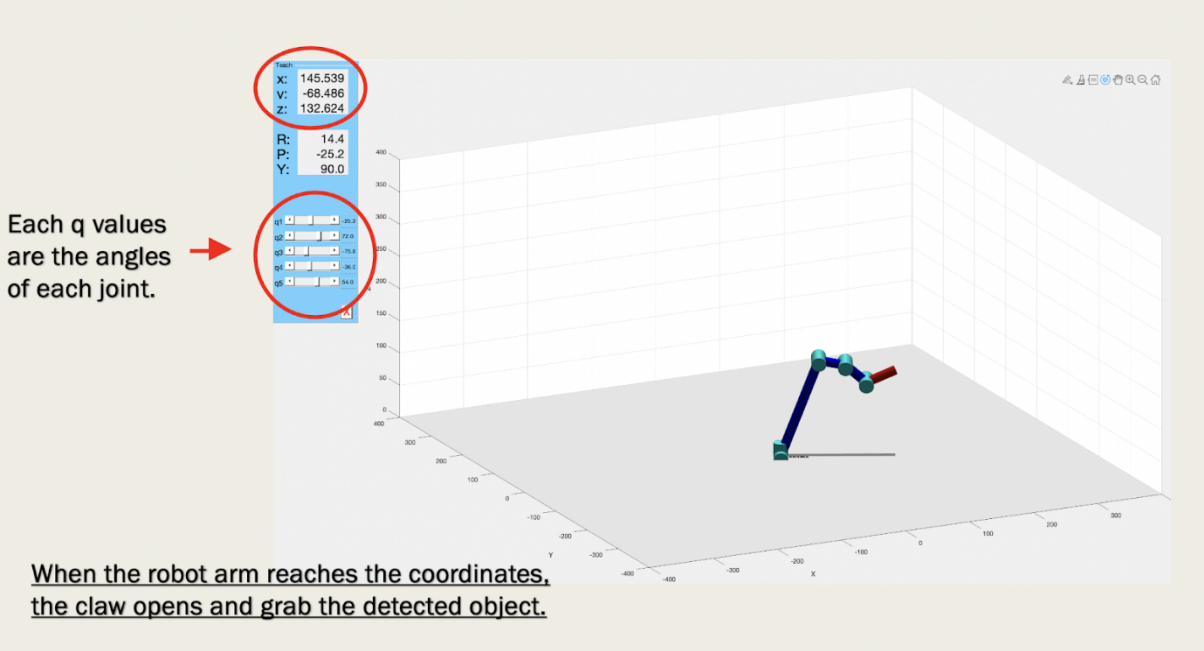

Figure 19: The robotic arm end effect reaches the desired position.

8.2 Reception and deconstruction of Debris at the factory

Once the space tug has delivered the debris to the factory entrance the debris is passed to the entrance robots for analysis. Computer vision is needed to identify the debris shape and constituent parts. This requires machine learning and AI techniques as although many defunct satellites might be of a standard design, each debris satellite may be in different condition, e.g. varying impact holes, missing or damaged parts, varying surface condition etc. In that way an individual deconstruction plan is developed for each debris object. This includes: (i) identification of large items, e.g. solar panels,)ii) where the fixings are that should be removed, (iii) where to hold the debris at each stage of the deconstruction process and (iv) what tools and number of arms the robots need to have. The robots have the capability of changing their tools at the end of their arms.

8.2.1 Debris Shape Detection

As an example, consider the identification and deconstruction of a cube-type satellite debris object. The satellite can be break down into different sections:

1 Solar panels and louvers
2 External objects such as antenna, communications dish.
3 The front panel where sensor/camera equipment operate from.
4 The back panel- the back of satellite where some propulsion thruster may be attached.
5 Side panels
6 The equipment inside the satellite including electronics, power sources, heaters.

Therefore, with the same method used above, the model is trained again to detect the parts mentioned above, starting with the external parts (Figure 20). The disassembly process would depend on the debris design but due to the popularity of communication satellite constellations, a procedure favouring these types of satellites would be practical. Care would be needed to deposit all

parts of the debris, down to the smallest fastener as debris floating unchecked with the factory would pose a danger to the operation of the equipment inside.

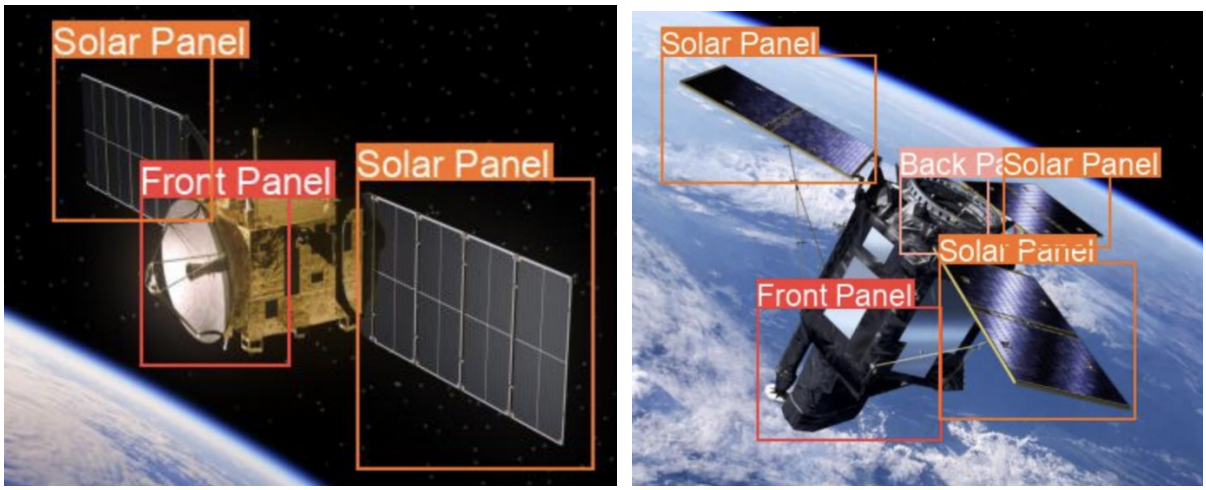

Figure 20a, b: Different parts detected.

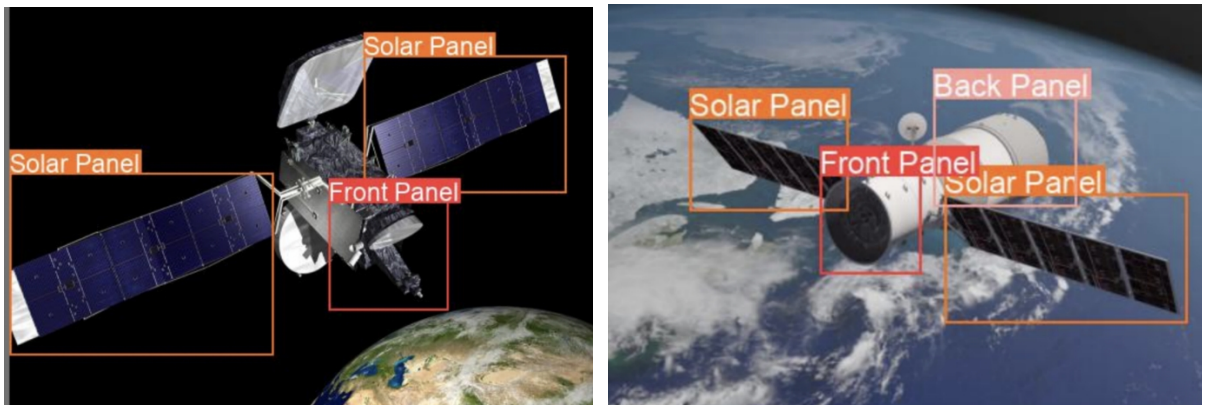

Figure 20c, d: Different parts detected.

8.2.2 Debris metal categorisation

Identification of material composition is a challenge. Given prior information, e.g. if manufacturers were required to supply a detailed description of each part, fixing and materials, then deconstruction would be more straight-forward. However without this information, identification in situ is needed. Once the composition is assessed, it can be decided what parts are to be utilised immediately in the other parts of the factory and what parts are to be stored, e.g. placing reclaimed gold material in one storage bin and aluminium in another.

One approach would be to include metal sensors into an end tool part for a robot arm to use (Figure 13). Krüger and Ewald (2010) proposed an imaging method for the recognition of metal detector data from an inductive sensor to capture precise information on the metal. The values detected by the sensors depend on the type, characteristics, size and geometry of the material of object (e.g. ipf electronic, 2016). Their imaging process was articulated by a convolution function to produce the reconstructed image function of the object geometry F(x,y) with an aperture function H(x,y) and an additive noise term or raw data function G(x,y). F is defined by the quotient (G/H). With the convolution method, object geometry is properly identified and is compared with raw data to obtain accurate information of the material with the correct correction factor. Inductive sensors work by applying a magnetic force to detect the object. Different metals can be detected by inductive sensor by different distances. For example, if you refer to the correction factor, steel is 1.0, which means

depending on its dataset, steel always can be detected at the factor of 1.0. The factor is set and its value provided by the manufacturer. Other metals can be detected with different factors (usually 0.7 for stainless steel, 0.5 for brass, 0.4 for aluminium, 0.3 for copper). There is also a dependency on distance. For example if a 5 cm distance is 1.0 factor for the sensor, then if a steel object is 3cm away from the sensor, the sensor will not send a signal, since it cannot detect steel at 3cm; it can only detect it 5cm away. Inductive sensors are also affected by the shape of metal. For example, different shapes of steel may be detected in different distance, that might be inaccurate to factor 1.0. Therefore, it is necessary to have the distance and shape information known so that comparison can be made when in space. The correction factor is an important assistance to comprehend the correct value of the sensor data. A sensor would be connected to any microcontroller in an ADC (Analogue to Digital Signal Converter) module and values are recorded on the different materials.

8.4 Production of recycled material for Additive Manufacturing.

Once the challenge of disassembling debris has been achieved, the resultant parts are either stored for future use or passed to the next stage of the factory where the metals are melted in order to reform and create new products. Although there are many methods for 3d printing, it is important to ensure that there is no opportunity of any dust moving from the additive manufacturing area to other parts of the space factory. Thus the chosen approach here for the recycling is to create metal wire which is easily stored, can be made in a number of diameters, is easily transportable and can be fed to the 3d printers.

The debris would be melted using electromagnetic levitation techniques where the applied fields are used to hold the metal in place and to shape the metal. The idea that metals can be melted and fabricated in microgravity, with the opportunity of producing more enhanced metal products has been explored since Wuenscher (1969).

The chosen debris metal is fed into the coil area to be melted where the electromagnetic field holds it in place initially. The transition from a molten ball of metal to wire is then effected by the heating of the field. At this stage the second electromagnetic field is switched on. The aim of this second field is to shape the metal by thinning it out so that a long train can be created. As the metal is drawn away from the original debris metal pool, it is formed into a constant diameter. In order to create a continuous process the amount of debris fed to the levitating (or controlling coils) must be the same as the amount of wire drawn out at the end of the process. The length of this part of the space factory must be sufficient for the wire to be held in place until the end has cooled enough to start the spooling process which continues until all the metal has been recycled.

For this project the UWE team (has been developing the process through the use of the software Elmer, OpenFoam and the EOF library to assist the multiphysics connection. This follows the work of

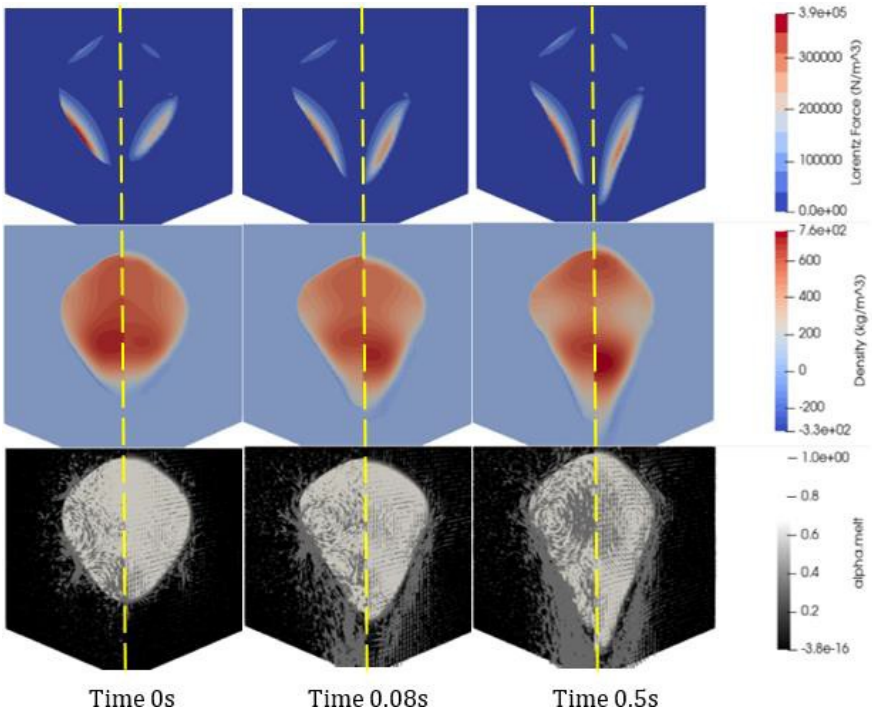

Figure 21: Showing how the shape of a molten metal blob changes with time. For each of the nine pictures the left hand picture is simulated using Elmer-Openfoam, whereas the right hand picture is taken from the validated results of Li et al. (2003). Detailing Lorentz force (top), density (middle) and Internal flow (bottom).

8.5 Additive manufacturing in space

Additive manufacturing will be a major contributor to the production of space manufactured items. The versatility of the approach in creating objects of plastic, resin, metal and composites makes it valuable in that the raw materials can be launched into space and the items created on site. This will reduce the number of launches needed. It will also provide a means of making an object when it is needed whereas waiting for a launch delivery could take weeks or months. The restriction with 3D printing is that the raw material should not be in powder form as there is the danger of powder floating across the space factory and lodging in machinery where disruptions would occur. Plans are in place for printing a Moon base, as well as printing food for Astronauts (aniwaa, 2022).

8.6 Construction in Space

The design of structures in space requires careful consideration and the testing of various concepts in order to achieve an optimal design. One of the intended products of the space factory would be the printing of panels to assemble into storage pods, In the initial stages these pods would be sent up from Earth, either complete or in sections to be connected. The pods could be constructed in a variety of ways including cross-bars for greater strength (Figure 22a, left) or just connector bars of larger radius (Figure 22b, right). The cuboid design would be developed as a set of possible volumes: (2 m x2 m x 2 m) and then say (4x4x4) and (8x8x8). The modular approach would benefit the extension of the space factory by adding in additional cylindrical sections.

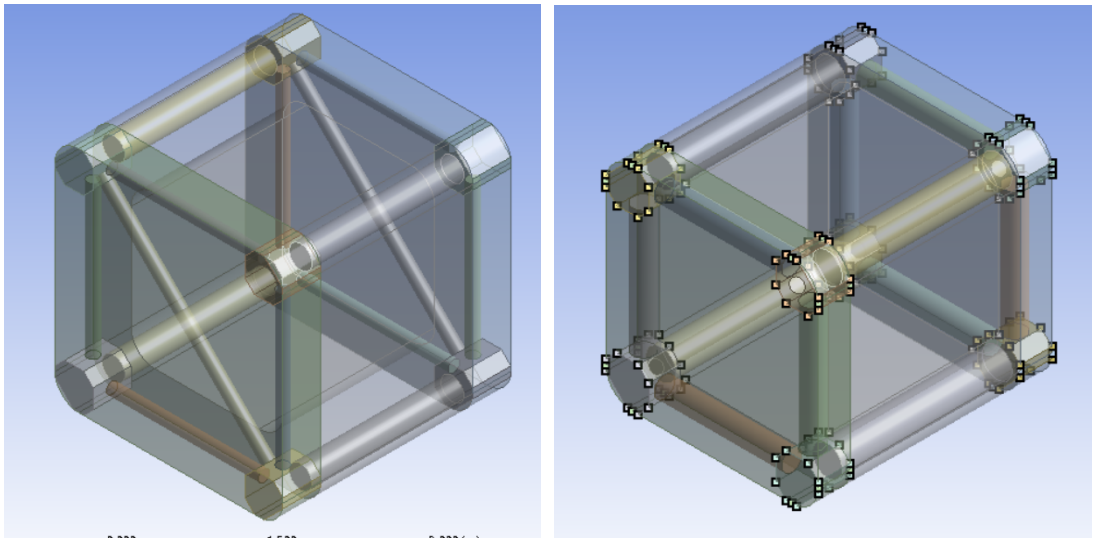

Figure 22: various design for a storage unit attached to the space factory (ANSYS, designed by Ahmed Alshobokshy) (a) cross-bar supports, (b) thicker cross-bars

The structural integrity of the designs was investigated using the software ANSYS Mechanical. An example of the results is shown in Figures 23 and 24. The storage pods come in a number of standard sizes, e.g. (1m x 1m x 1m), (2m x 2m x 2m) or (8m x 8m x 8m). In the examples shown here, the cylindrical supports have a diameter of (1/8) the maximum width. Note the higher stresses and skewness at the joints and corners.

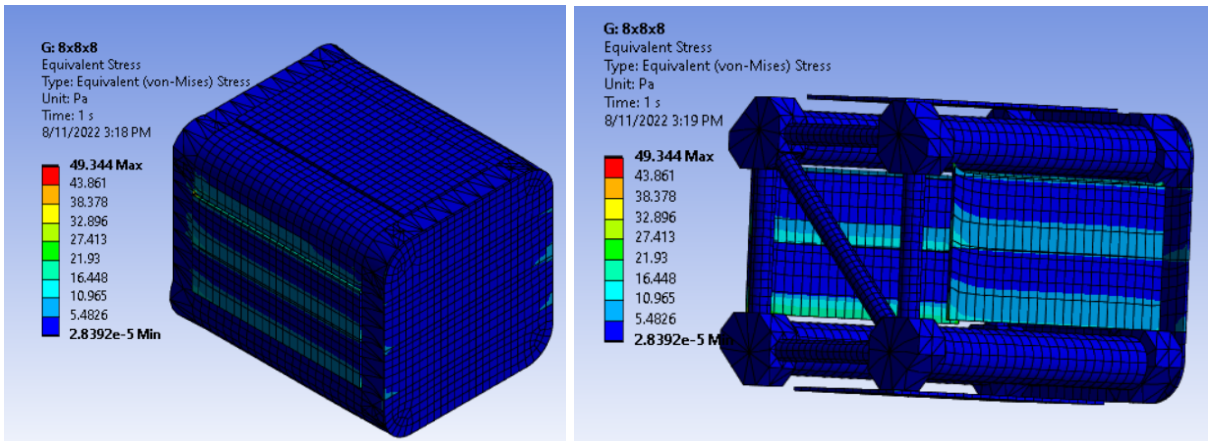

Figure 23 Example showing the stress distribution on one of the storage pods (ANSYS Mechanical)

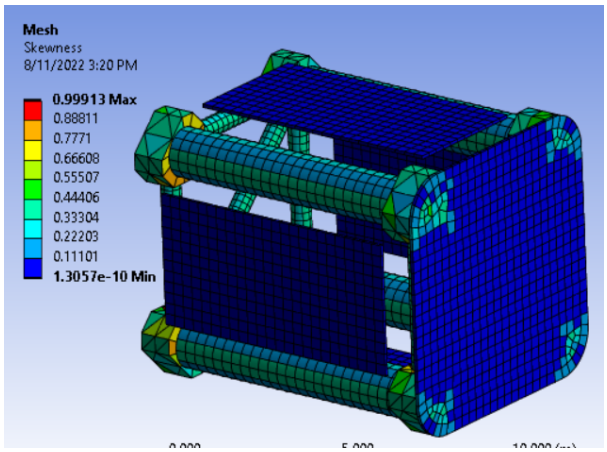

Figure 24 illustrates the skewness on the storage pod (ANSYS Mechanical)

Similarly for the construction in space of trusses to attach e.g. solar panels would result in arrays as in Figure 25. The aim would be for the connectors and rods to be 3D printed within the factory. Tethered robots or space tug robots would then take the parts from the factory and assemble the structure in-situ in space as required.

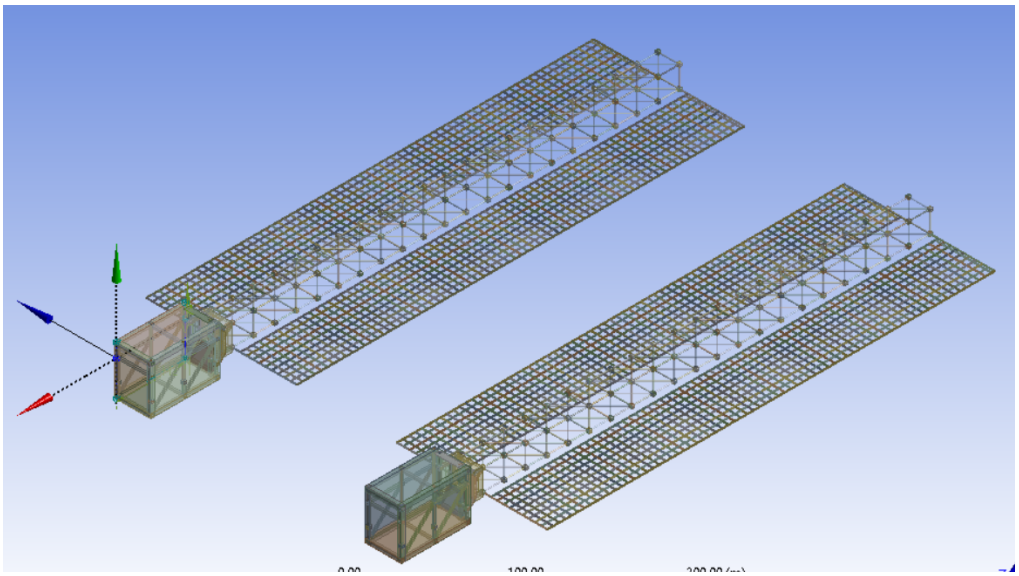

Figure 25: Conceptual space storage pods, each with a truss structure of recycled 3D rods to which solar panels are attached (Ahmed Alshobokshy)

8.7 Other products from the Space Factory

Some of the other potential products from the space factory are new metal alloys and metal matrix alloys, using the container-less magnetic field levitation approach. In addition, one useful type of product are aeroshells such as a space shield and decelerator. A typical aeroshell is composed of an aluminium honeycomb structure with graphite-epoxy sheets. The object being protected is either put inside the blunted cone or travels behind it. Such a rigid structure could be 3D printed in space for use to protect the space factory or protect the delivery of new products either across low Earth orbit (so that it would absorb much of the impact of small shards of space debris acting as a Whipple shield) or for delivery of products back to Earth using a decelerator. Decelerators are often more complex than space shields, being composed of a succession of carbon fibre tubes or tori (Figure 25) which can modify their shape to aid deceleration as they travel down through an atmosphere. The composite structure can be many times stronger than steel.

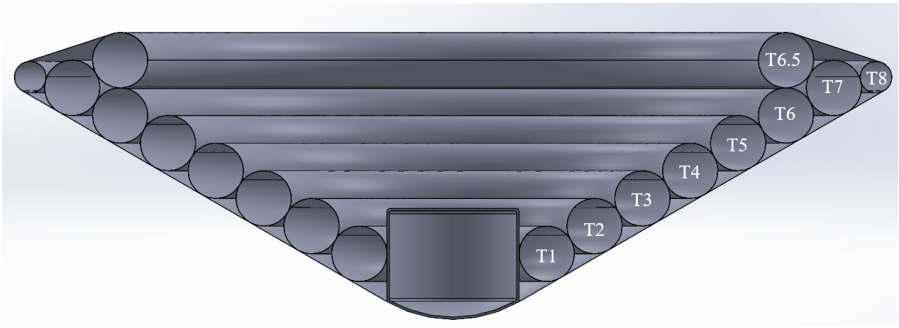

Figure 26 Design for a typical stacked tori blunted cone decelerator (based on Kazemba et al. 2013)

As an example, the decelerator in Figure 26 was tested for atmospheric entry where the deformation was tested as a function of altitude (the decelerator is travelling such that its nose is

leading into the atmosphere. The resulting deformation is shown in Figure 27 and the flowfield around the vehicle as it decelerates to Mach 5 is shown in Figure 28.

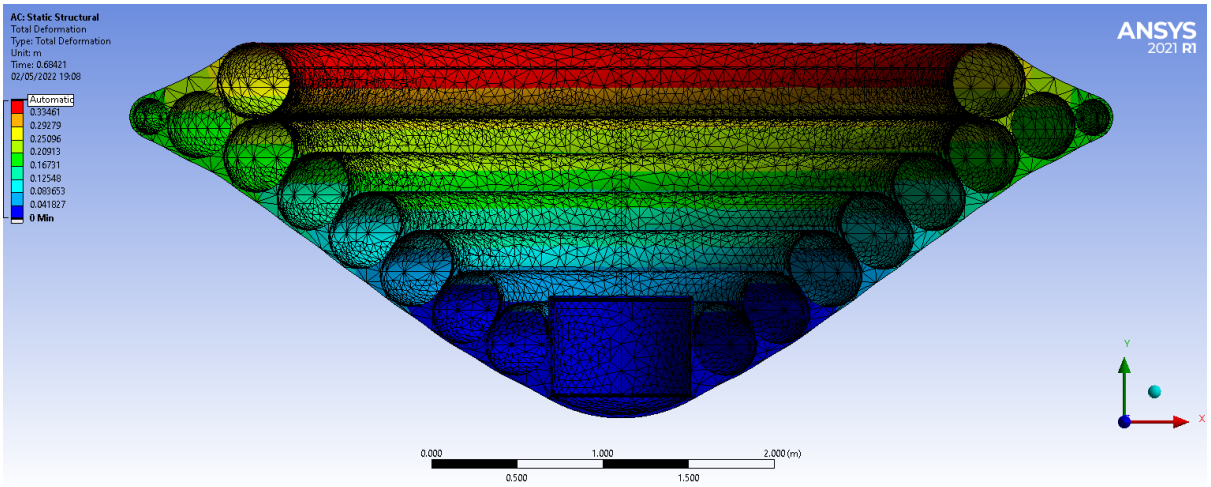

Figure 27 Deformation in the decelerator showing small changes of a mm for a vehicle of maximum diameter 6 metres. (Taisia Bennett using Software: ANSYS Mechanical)

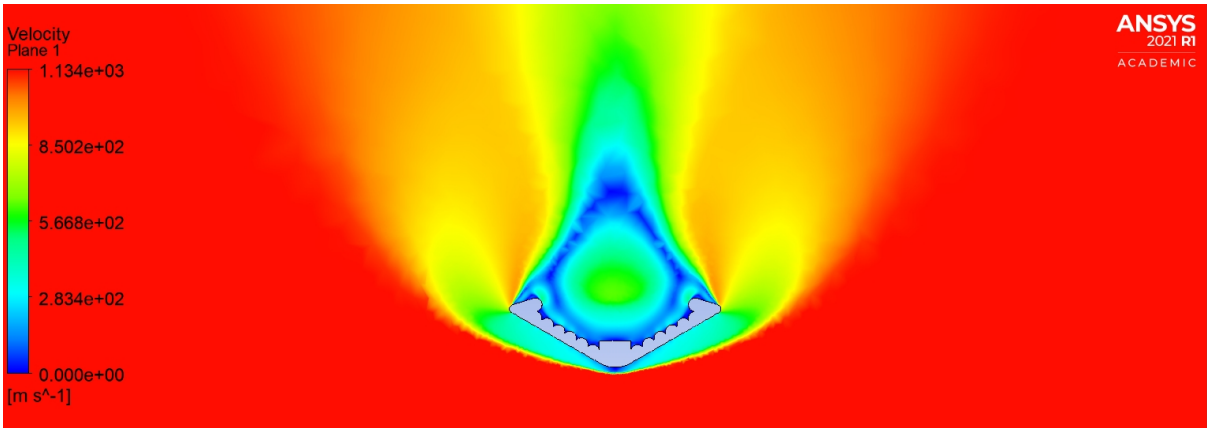

Figure 28 Cross-sectional flowfield around the shield from Figure 27 as it decelerates through the atmosphere (the shield is travelling downwards). The example shown has the shield at Mach 5. The colours indicate the complex pattern in the reduction in speed around the vehicle especially close to the back (Taisia Bennett using software ANSYS Fluent).

9. Conclusions

The development of a sustainable, manoeuvrable, solar-powered space vehicle of multi-mission capability would transform space operations, debris mitigation, space commerce and exploration. The ability to be able to safely clear the majority of space debris mass would significantly lower the risks faced by current satellite and launch providers. The vehicle would also be a workhouse in Low Earth orbits enabling better control of existing spacecraft, a longer life and reducing the need for future spacecraft to carry fuel and orbital positioning engines.

The space factory is a longer term development but essential for a continual presence in space. Being able to manufacture what is needed for space, in-space, would substantially reduce the amount of items sent into space. If some of that can be done through recycling old spacecraft , then the benefits of sustainability come not just in terms of reduced cost and increased convenience but set a standard to which future launch and service providers need to reach.

Space manufacturing will enable a different set of products and technologies. New materials, pharmaceuticals, and electronics are just some of the benefits that will be brought back to Earth. The space manufacturing factories will also provide the base for future mission development, e.g. creating habitats for the Moon, processing the material from space mining and developing solar power installations to support future space stations.

The authors believe that the growth rate of activities in space will increase exponentially. Investment in, and wise management of, such space technologies will likely provide not just sizeable profits but substantial benefits for human-kind in terms of health, security, society and environment.

10. References

Adams, A. and Willett, N. (2010) *Depth of field* [online]. Available from: https://graphics.stanford.edu/courses/cs178-10/applets/dof.html [Accessed 10 Aug 2022]

Airbus, 2022, In space manufacturing and assembly, https://www.airbus.com/en/newsroom/news/2022-05-in-space-manufacturing-and-assembly (last accessed 29.08.2022)

Alcubierre, Miguel, 1994, "The warp drive: hyper-fast travel within general relativity." *Classical and Quantum Gravity* 11.5 (1994): L73.

Anderson, Joe (2021) "MISSION EXTENSION VEHICLE (MEV) Award-Winning Satellite-Life-Extension Servicing Vehicle", available at: https://www.northropgrumman.com/wp-content/uploads/Mission-Extension-Vehicle-MEV-fact-sheet.pdf (last accessed 23/08/2022)

Aniwaa, 2022, https://www.aniwaa.com/guide/3d-printers/3d-printing-for-space/ Last accessed 16.09.2022

Barnhart, David & Sullivan, Brook R., 2012, Economics of Repurposing In Situ Retired Spacecraft Components, *AIAA Space 2012 Conference & Exposition.*

Bondarenko, Daniel, Gabbar, Hossam A and Stoute, C.A. Barry, 2017, Engineering design of plasma generation devices using Elmer finite element simulation methods. *Engineering Science and Technology, an International Journal*, 20(1):160–167.

Brieda, Lubos, 2018, Model for steady-state fully kinetic ion beam neutralization studies. *IEEE Transactions on Plasma Science*, 46(3):556–562.

Brieda, Lubos and Keidar, Michael, 2012, Development of the Starfish plasma simulation code and update on multiscale modeling of hall thrusters. In *48th AIAA/ASME/SAE/ASEE Joint Propulsion Conference & Exhibit*, page 4015.

Chintarungruangchai, P. and Jiang, I., 2019, Detecting Exoplanet Transits through Machine-learning Techniques with Convolutional Neural Network [online]. Available from: https://doi.org/10.1088/1538-3873/ab13d3 [Accessed 02 Aug 2022]

Colorado, 2021, ME Team Awarded NASA In-Space Recycling Project. https://mechanical.mines.edu/me-nasa-inspace-recycling-project/, (last accessed 04.09.2022)

Corke, P.(2022) *Robotics Toolbox* [online]. Available from: https://petercorke.com/toolboxes/robotics-toolbox/ [Accessed 10 Aug 2022].

ESA, 2019, "*ESA commissions world's first space debris removal",* https://www.esa.int/Safety_Security/Clean_Space/ESA_commissions_world_s_first_space_debris_removal

ESA, 2021, "Space debris by the numbers*"*, https://www.esa.int/Safety_Security/Space_Debris/Space_debris_by_the_numbers , 2021

ESA, 2022, Terrae Novae 2030+ Strategy Roadmap, https://esamultimedia.esa.int/docs/HRE/Terrae_Novae_2030+strategy_roadmap.pdf (last accessed 29.08.2022)

Ferreira, Eugenio et al., 2021 "Airbus's vision for In-Orbit Servicing", available at: https://indico.esa.int/event/321/contributions/6332/contribution.pdf (last accessed 23.08.2022)

Fletcher,K. (Ed.),"Space Operations Space Debris, the ESA approach", *ESA Publication*, 2017

Forshaw, J. L. Aglietti, G. S. Salmon, T. Retat, I. Roe, M. Burgess, C. Chabot, T. Pisseloup, A. Phipps, A. Bernal, C. Chaumette, F. Pollini, A. Steyn, W. H. m 2017, "Final payload test results for the RemoveDebris active debris removal mission", *Acta Astronautica, Volume 138.*

Forshaw, J., 2018, "Astroscale's ELSA-d Mission and ESA Support Mechanisms", ESA Clean Space, ESTEC, 2018

Foust, Jeff (04/02/2019), "Rethinking satellite servicing", available at: https://www.thespacereview.com/article/3653/1 (last accessed 23.08.2022)

Github (2022) *YOLOv5* [online]. Available from: https://github.com [Accessed 27 July 2022].

Intelsat Corporate Communications, 2019, available at**:** https://www.intelsat.com/newsroom/intelsat-29e-satellite-failure/ (last accessed 23/08/2022)

ipf electronic (2016) Inductive sensors. Available from: https://www.tme.eu/Document/49c8c097f17582ba961358e6d754f63e/INDU1150_en.pdf [Accessed 8 Aug 2022].

ISECG, 2018, The ISECG Global Exploration Roadmap, Published by NASA, https://www.globalspaceexploration.org/wordpress/wp-content/isecg/GER_2018_small_mobile.pdf (last accessed 29.08.2022)

Johnson, Michele, 2017, available at: https://www.nasa.gov/feature/ames/kepler/nasa-ends-attempts-to-fully-recover-kepler-spacecraft-potential-new-missions-considered (Last accessed 23.08.2022)

Kazemba, C.D., Tran, K., Quach, B., Kushner, L.K., Cassell, A., Li, L., Braun, R., Littell, J., Van Norman, J., Johnson, R.K. and Hughes, S.J., 2013. Determination of the deformed structural shape of HIADs from photogrammetric wind tunnel data. In *AIAA Aerodynamic Decelerator Systems (ADS) Conference* (p. 1286).

Kessler, Donald J., 2009."The Kessler Syndrome", available at: http://webpages.charter.net/dkessler/files/KesSym.html (last accessed 23/08/2022)

Klemz, Nicholas, 2019, “An apparatus for generating a force”, patent, https://www.ipo.gov.uk/p-ipsum/Case/PublicationNumber/GB2588415 (last accessed 19.08.2022)

Krüger, H. and Ewald, H. (2010) *2D image reconstruction from blurred and disturbed multi parameter measurements at the example of an inductive metal detector* [online]. SENSORS, 2010 IEEE, 2010, pp. 1325-1328, doi: 10.1109/ICSENS.2010.5690565. Available from: https://ieeexplore.ieee.org/document/5690565/ [Accessed 12 Aug 2022].

Leap, J.Z., 2022, The Methodology of the Implementation of Robotics in Building a Space Factory. University of the West of England Internal Report.

Li, S., Li, J., Hao, Q., Kou, H., Li, J. and Fu, H., 2003. Research on the dual-frequency electromagnetic shaping of liquid metal. *Journal of Materials Processing Technology*, 137(1-3), pp.204-207.

Morgan Stanley Space Team, 2022, A New Space Economy on the Edge of Liftoff, https://www.morganstanley.com/Themes/global-space-economy (last accessed 29.08.2022)

National Research Council Committee on Space Debris, 1995, “Orbital Debris, A Technical Assessment”, National Academy Press

Ning, W. (2021) *Inverse Kinematics* [online]. Robot Control System UFMFVF-30-2. Available from: https://blackboard.uwe.ac.uk [Accessed 10 Aug 2022]

OECD, 2020, Space Sustainability. *The Economics of Space Debris in perspective*, OECD Science, Technology & Industry Policy Paper No. 87, https://www.oecd-ilibrary.org/docserver/a339de43-en.pdf?expires=1624818770&id=id&accname=guest&checksum=83B9553DB743AEA0F907223570AD25AE (last accessed 17.06.2021)

Onishi, Y., Yoshida, T., Kurita, H., Fukao, T., Arihara H. and Iwai, A. (2019) *An automated fruit harvesting robot by using deep learning.* ROBOMECH Journal [online]. J6, 13. Available from: https://doi.org/10.1186/s40648-019-0141-2 [Accessed 27 July 2022].

Panofsky, Wolfgang and Phillips, Melba, 1962, “Classical Electricity and Magnetism” by 2nd edition, Addison-Wesley.

Råback, Peter, Malinen, Mika, Ruokolainen, Jiha, Pursula, Antti and Zwinger, Thomas, 2013, Elmer models manual. *CSC–IT Center for Science, Helsinki, Finland*.

SatCatalog, 2022, “S400-12 Biprop Thruster”, available at: https://www.satcatalog.com/component/s400-12-biprop-thruster/ (last accessed 23.08.2022)

Tajima, T., 2018, Computational plasma physics with applications to fusion & astrophysics. *CRC Press.*

Thompson, A., Toomer, C.A., & Bolouri, A., 2018, A Space Recycling Plant to reduce Orbital Debris, *Report to the UK Space Agency.*

Warwick, Graham, 2019, Spotlight: Satellite Servicing, available at: https://aviationweek.com/defense-space/space/spotlight-satellite-servicing (last accessed 23.08.2022)

Weinzierl, Matt & Sarang, Mehak, 2021, The Commercial Space Age is Here, Harvard Business Review, https://hbr.org/2021/02/the-commercial-space-age-is-here (last accessed 29.08.2022)

Wuenscher, H.F.W (1969) space manufacturing unique to zero gravity environment. https://ntrs.nasa.gov/api/citations/19700017984/downloads/19700017984.pdf [Accessed 26th February 2022].

Appendix 1

Presented here are some well-known equations of classical electricity and magnetism. They are for reference only.

Maxwell's equations

Name	Integral form	Differential form
Gauss' law	$\oiint \mathbf{E} \cdot \mathrm{d}\mathbf{S} = \frac{1}{\varepsilon_0} \iiint_\Omega \rho \, \mathrm{d}V$	$\nabla \cdot \mathbf{E} = \frac{\rho}{\varepsilon_0}$
Gauss' law for magnetism	$\oiint \mathbf{B} \cdot \mathrm{d}\mathbf{S} = 0$	$\nabla \cdot \mathbf{B} = 0$
Faraday's and Lenz's laws	$\oint_{\partial\Sigma} \mathbf{E} \cdot \mathrm{d}\boldsymbol{\ell} = -\frac{\mathrm{d}}{\mathrm{d}t} \iint_\Sigma \mathbf{B} \cdot \mathrm{d}\mathbf{S}$	$\nabla \times \mathbf{E} = -\frac{\partial \mathbf{B}}{\partial t}$
Ampere's circuital law with Maxwell's addition (displacement current)	$\oint_{\partial\Sigma} \mathrm{B} \cdot \mathrm{d}\boldsymbol{\ell} = \mu_0 \left(\iint_\Sigma \mathrm{J} \cdot \mathrm{d}\mathbf{S} + \varepsilon_0 \frac{\mathrm{d}}{\mathrm{d}t} \iint_\Sigma \mathrm{E} \cdot \mathrm{d}\mathbf{S} \right)$	$\nabla \times \mathbf{B} = \mu_0 \left(\mathbf{J} + \varepsilon_0 \frac{\partial \mathbf{E}}{\partial t} \right)$

Electromagnetic stress-energy tensor

$$T^{\mu\nu} = \begin{bmatrix} \frac{1}{2}\left(\epsilon_0 E^2 + \frac{1}{\mu_0} B^2\right) & \frac{1}{c} S_\mathrm{x} & \frac{1}{c} S_\mathrm{y} & \frac{1}{c} S_\mathrm{z} \\ \frac{1}{c} S_\mathrm{x} & -\sigma_{\mathrm{xx}} & -\sigma_{\mathrm{xy}} & -\sigma_{\mathrm{xz}} \\ \frac{1}{c} S_\mathrm{y} & -\sigma_{\mathrm{yx}} & -\sigma_{\mathrm{yy}} & -\sigma_{\mathrm{yz}} \\ \frac{1}{c} S_\mathrm{z} & -\sigma_{\mathrm{zx}} & -\sigma_{\mathrm{zy}} & -\sigma_{\mathrm{zz}} \end{bmatrix},$$

$$\mathbf{S} = \frac{1}{\mu_0} \mathbf{E} \times \mathbf{B},$$

$$\sigma_{ij} = \epsilon_0 E_i E_j + \frac{1}{\mu_0} B_i B_j - \frac{1}{2}\left(\epsilon_0 E^2 + \frac{1}{\mu_0} B^2\right) \delta_{ij}$$